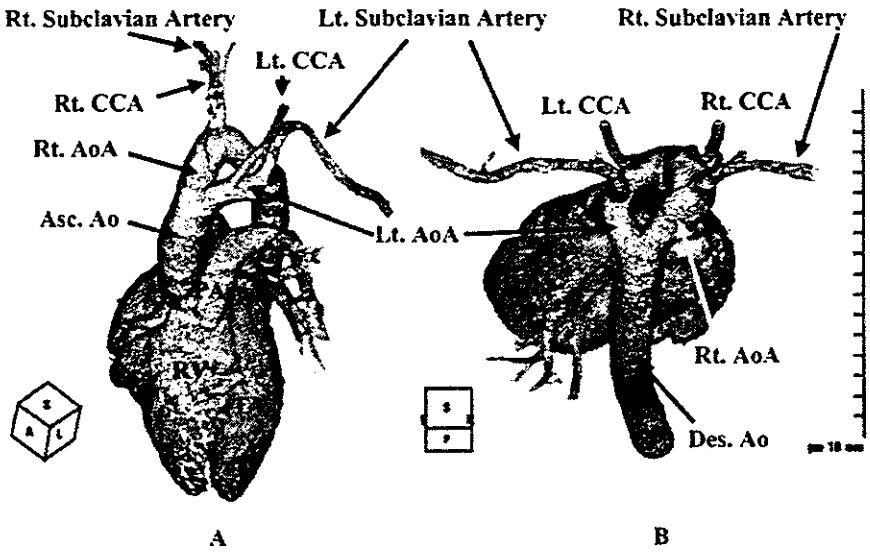

Figure 2. Three-dimensional volume rendering image of enhanced multislice CT from the left superior anterior view (A) and from the superior posterior view (B) revealed double aortic arches (AoA) separated at the distal portion of the ascending aorta (Asc. Ao) (A) and joined at the proximal portion of the descending aorta (Des. Ao) (B). The right (rt.) subclavian artery and right common carotid artery (CCA) originated separately from the right aortic arch (rt. AoA), and the left (lt.) subclavian artery and left CCA originated from the left aortic arch (lt. AoA). PA indicates pulmonary artery; RV, right ventricle; and LV, left ventricle.

THE JOURNAL OF BIOLOGICAL CHEMISTRY
© 2004 by The American Society for Biochemistry and Molecular Biology, Inc.

Vol. 279, No. 39, Issue of September 24, pp. 41095–41103, 2004
Printed in U.S.A.

Diphtheria Toxin-induced Autophagic Cardiomyocyte Death Plays a Pathogenic Role in Mouse Model of Heart Failure*

Received for publication, December 1, 2003, and in revised form, May 20, 2004
Published, JBC Papers in Press, July 22, 2004, DOI 10.1074/jbc.M313084200

Hiroshi Akazawa‡§, Shinji Komazaki¶, Hiroaki Shimomura‖, Fumio Terasaki‖, Yunzeng Zou‡, Hiroyuki Takano‡, Toshio Nagai‡, and Issei Komuro‡**

From the ‡Department of Cardiovascular Science and Medicine, Chiba University Graduate School of Medicine, 1-8-1 Inohana, Chuo-ku, Chiba 260-8670, Japan, the ¶Department of Anatomy, Saitama Medical School, 38 Morohongou, Moroyama, Iruma 350-0495, Japan, ‖The Third Division, Department of Internal Medicine, Osaka Medical College, 2-7 Daigaku-machi, Takatsuki 569-8686, Japan, and the §Foundation for Biomedical Research and Innovation, 6-1, Minatojima Nakamachi, Chuo-ku, Kobe 650-8543, Japan

It is still not clear whether loss of cardiomyocytes through programmed cell death causes heart failure. To clarify the role of cell death in heart failure, we generated transgenic mice (TG) that express human diphtheria toxin receptor in the hearts. A mosaic expression pattern of the transgene was observed, and the transgene-expressing cardiomyocytes (17.3% of the total cardiomyocytes) were diffusely scattered throughout the ventricles. Intramuscular injection of diphtheria toxin induced complete elimination of the transgene-expressing cardiomyocytes within 7 days, and ~80% of TG showed pathophysiological features characteristic of heart failure and were dead within 14 days. Degenerated cardiomyocytes of the TG heart showed characteristic features indicative of autophagic cell death such as up-regulated lysosomal markers and abundant autophagosomes containing cytosolic organelles like cardiomyocytes of human dilated cardiomyopathy. The heart failure-inducible TG are a useful model for dilated cardiomyopathy, and provided evidence indicating that myocardial cell loss through autophagic cell death plays a causal role in the pathogenesis of heart failure.

Cardiomyocyte death is observed in a number of pathological conditions such as ischemic or dilated cardiomyopathy, hypertensive heart disease, and aging (1). Oncosis has been recognized to be a principal mechanism of myocardial cell death, but during the last decade, much emphasis has been put on the importance of apoptosis on the basis of detectable apoptotic cardiomyocytes in animal and human models of heart failure (2). Recently, autophagic cell death (ACD)[1] has been demonstrated as another type of myocardial cell death in human failing hearts (3–7). Although a decline in pumping capacity initiated by cardiomyocyte loss is supposed to induce ventricular remodeling and finally results in symptomatic heart failure (8), there still remains a controversy over the pathogenic role of cell death in progression of heart failure (9, 10). An intractable problem that hampers mechanistic insights is the low occurrence of myocardial cell death in failing hearts, although it differs strikingly according to the models examined and technical specificity (2, 8). Furthermore, in human hearts, most samples were obtained from patients with end-stage heart failure who underwent heart transplantation and thus it remains unknown whether myocardial cell death occurs persistently from an early stage and is causative to progression of heart failure (8). To circumvent these obstacles, we established an inducible heart failure mouse model utilizing diphtheria toxin (DT)-mediated cell ablation, in which a given number of cardiomyocytes are arbitrarily and synchronously ablated, and prospective and serial analysis is available.

DT is a two-peptide protein consisting of fragments A (DT-A) and B (DT-B) produced by *Corynebacterium diphtheriae* (11). DT binds to the DT receptor on the cell surface through DT-B and is internalized into acidic endocytic vesicles, which allows release of catalytic DT-A into the cytoplasm (12). DT-A exerts its cytotoxicity by ADP-ribosylating elongation factor 2 and thereby inhibiting protein synthesis in infected cells (13). DT receptor has been identified as a precursor of heparin-binding EGF-like growth factor (pro-HB-EGF) (14, 15). Intriguingly, DT cannot bind to rodent pro-HB-EGF because of substitution of amino acids required for DT binding, whereas primate pro-HB-EGF acts as a functional DT receptor (16). Therefore, specific cells in mice are ideally sensitized to DT by forced expression of human pro-HB-EGF (17).

To enable cardiac-specific cell ablation, we generated transgenic mice (TG) expressing human pro-HB-EGF in the hearts under the control of *α-myosin heavy chain* promoter. Administration of DT induced ablation of transgene-expressing cardiomyocytes, and subsequently symptomatic heart failure. In this mouse model of heart failure, autophagy but not apoptosis was the mechanism of cardiomyocyte death. Autophagy is a dynamic process and intracellular constituents are sequestered by membranes and subsequently degradated or recycled in lysosome or vacuole (18–20). In this sense, autophagy is involved in maintaining cellular homeostasis and turnover in physiological conditions. However, a growing body of evidence suggests that autophagy is implicated in execution of pro-

* This work was supported in part by grants from the Japanese Ministry of Education, Science, Sports, and Culture of Japan, Japan Health Sciences Foundation, Takeda Medical Research Foundation, Takeda Science Foundation, Uehara Memorial Foundation, Kato Memorial Trust for Nambyo Research, an the Japan Medical Association (to I. K.) and a Japanese Heart Foundation/Pfizer Japan Grant on Cardiovascular Disease Research (to H. A.), and the New Energy and Industrial Technology Development Organization. The costs of publication of this article were defrayed in part by the payment of page charges. This article must therefore be hereby marked "*advertisement*" in accordance with 18 U.S.C. Section 1734 solely to indicate this fact.

** To whom correspondence should be addressed. Tel.: 81-43-226-2097; Fax: 81-43-226-2557; E mail: komuro-tky@umin.ac.jp.

[1] The abbreviations used are: ACD, autophagic cell death; BNP, brain natriuretic peptide; DT, diphtheria toxin; DT-A, DT fragment A; DT-B, DT fragment B; LAMP-1, lysosome-associated membrane protein-1; MCP-1, macrophage chemoattractant protein-1; MLP, muscle LIM protein; pro-HB-EGF, precursor of heparin-binding epidermal growth factor-like growth factor; SERCA2, sarcoplasmic reticulum calcium-ATPase 2; TG, transgenic mice; WT, wild-type mice.

grammed cell death and is closely linked to several pathological conditions (21–23). Our model of experimentally induced heart failure provided direct evidence that myocardial cell loss through ACD causes heart failure, and will be useful to dissect the molecular mechanisms underlying structural and functional changes in heart failure.

EXPERIMENTAL PROCEDURES

Generation of Transgenic Mice—Human *pro-HB-EGF* cDNA (gift from A. Ullrich, Max-Planck-Institute of Biochemistry, Martinsried, Germany) was subcloned into the α-myosin heavy chain promoter-containing expression vector (gift from J. Robbins, Children's Hospital, Cincinnati, OH). The 6.9-kb DNA fragment was microinjected as a transgene into pronuclei of eggs from BDF1 mice, and the eggs were transferred into the oviducts of pseudopregnant ICR mice. The transgene was identified by Southern blot and PCR analysis. All protocols using mice were approved by the Institutional Animal Care and Use Committee of Chiba University.

Administration of Diphtheria Toxin—Diphtheria toxin (Sigma) was reconstituted in 10 mM sodium phosphate buffer (pH 7.4) containing 5% lactose, and was administered by intramuscular injection.

Northern Blot and in Situ Hybridization Analysis—For Northern blot analysis, total RNA (20 μg) prepared from tissues were hybridized with cDNA probes. Probes for brain natriuretic peptide (*BNP*), skeletal α-actin, sarcoplasmic reticulum calcium-ATPase 2 (*SERCA2*), and *TNF-α* were previously described (24–26). Probes for macrophage chemoattractant protein-1 (*MCP-1*) and collagens (*Col1a2* and *Col3a1*) were gifts from K. Matsushima (Universitty of Tokyo, Tokyo, Japan) and S. Kim (Osaka City University, Osaka, Japan), respectively. Digoxygenin-labeled riboprobes were synthesized by using the 0.7-kb human *pro-HB-EGF* cDNA, and RNA *in situ* hybridization was performed as described previously (27).

Western Blot Analysis—Protein samples were fractionated by SDS-PAGE, and immunoblot analysis was performed as described previously (26, 28).

Transthoracic Echocardiography—Mice were anesthetized by intraperitoneal injection of a mixture of ketamine (100 mg/kg) and xylazine (5 mg/kg). Cardiac function was evaluated with echocardiography (SONOS 4500, Philips, Eindhoven, the Netherlands) using a 12-MHz transducer as described previously (26).

Histological Analysis and Immunohistochemistry—Hearts were fixed in 10% neutralized formalin and embedded in paraffin. Serial sections at 5 μm were routinely stained with hematoxylin-eosin for morphological analysis, and with Masson's trichrome for detection of fibrosis. For measurement of the myocyte cross-sectional area, semithin sections with silver staining were analyzed. Suitable cross-sections were defined as having round-to-oval cardiomyocyte sections and nearly round-shaped capillaries that perfused in the region. For immunohistochemistry, Vectastain ABC kit (Vector Laboratories, Burlingame, CA) was used to detect the primary antibodies. The sections were counterstained with hematoxylin.

Antibodies—The following antibodies were used: goat polyclonal anti-human HB-EGF (R&D Systems, Minneapolis, MN), anti-actin (20–33) IgG fraction of antiserum developed in rabbit (Sigma), mouse monoclonal anti-Ly-6G, mouse monoclonal anti-Mac-3, mouse monoclonal anti-CD3, mouse monoclonal anti-Bcl-xL, mouse monoclonal anti-cytochrome *c* (BD Pharmingen, San Diego, CA), rabbit polyclonal anti-caspase 3, mouse monoclonal anti-phospho-Bad, rabbit polyclonal anti-Bad (Cell Signaling, Beverly, MA), rabbit polyclonal anti-Bcl2, rabbit polyclonal anti-Bax, goat polyclonal anti-cathepsin D, rat monoclonal anti-lysosome-associated membrane protein-1 (LAMP-1), goat polyclonal anti-UBC2, goat polyclonal anti-E6-AP, goat polyclonal anti-UFD1 (Santa Cruz Biotechnology, Santa Cruz, CA), mouse monoclonal anti-COX I (Molecular Probes, Eugene, OR), mouse monoclonal anti-ubiquitin (Chemicon, Temecula, CA), and mouse monoclonal anti-E1 (Upstate, Charlottesville, VA).

Evaluation of DNA Fragmentation—TUNEL assay using paraffin sections was performed with an *in situ* apoptosis detection kit (Takara Biomedicals, Otsu, Japan). For agarose gel electrophoresis for DNA fragmentation, genome DNA (10 μg) was electrophoretically fractionated on a 1.5% agarose gel and stained with ethidium bromide as described previously (29). To induce apoptosis in spleens as positive controls, we injected lipopolysaccharide (40 mg/kg) (Sigma) in phosphate-buffered saline intraperitoneally into age-matched mice. Mice were sacrificed 12 h after lipopolysaccharide injection and spleens were excised (30).

Electronmicroscopy—Hearts were fixed in 3% paraformaldehyde, 2.5% glutaraldehyde, and 0.1 M cacodylate buffer (pH 7.4). After washing with the buffer solution and post-fixation in 1% OsO_4 and 0.1 M cacodylate buffer (pH 7.4), they were washed with the buffer solution, dehydrated using alcohol and acetone, and embedded in epoxy resin. Ultrathin sections were examined under the electron microscope (31).

Statistical Analysis—All values are expressed as mean ± S.E. Comparisons were made by Student's *t* test or one-way analysis of variance as appropriate. Values of $p < 0.05$ were considered statistically significant.

RESULTS

Inducible Myocardial Cell Ablation in TG Expressing Human DT Receptor in the Hearts—To confer DT sensitivity to cardiomyocytes in mice, we generated TG expressing human DT receptor, pro-HB-EGF, under the control of the α-myosin heavy chain promoter (Fig. 1*A*). Of two independent founder lines with successful germline transmission, one line was chosen for further analysis on the basis of transgene expression levels. By immunoblot analysis using an antibody specific for human pro-HB-EGF, we confirmed cardiac-specific expression of the transgene (Fig. 1*B*). *In situ* hybridization analysis using a specific riboprobe for human *pro-HB-EGF* further revealed a mosaic expression pattern of the transgene in the hearts (Fig. 1*C*). Expression of the transgene was scattered throughout the TG hearts, and the number of transgene-expressing cardiomyocytes was 17.3 ± 6.0% out of total cardiomyocytes.

To induce DT-mediated myocardial cell ablation, we administered DT by intramuscular injection to TG and wild-type mice (WT) at 10 weeks of age. When 5 mg/kg DT was administered, TG became lethargic and ~80% of TG died within 10 days after injection of DT, although WT appeared normal (Fig. 1*D*). Immunoblot analysis in combination with *in situ* hybridization analysis revealed that expression of human pro-HB-EGF in the TG hearts was significantly decreased on the next day of DT injection, and almost disappeared on the following day (Fig. 1*E*). After 7 days, transgene-expressing cardiomyocytes were undetected in the TG hearts, suggesting that they were completely ablated through DT-mediated cytotoxicity.

DT-mediated Myocardial Cell Loss Caused Heart Failure in Mice—We next examined the geometric, functional, and histological changes in the hearts caused by DT-mediated myocardial cell damages. Gross inspections of the TG hearts 7 days after DT injection showed global chamber dilatation with marked wall thinning and atrial thrombus (Fig. 2*A*), and the heart to body weight ratios were ~1.3-fold increased (Fig. 2*B*), whereas the mock-treated TG hearts and DT- or mock-treated WT hearts showed no geometric change (Fig. 2).

To evaluate cardiac function, we performed transthoracic echocardiographic examination. Seven days after injection, a ~1.3-fold increase in the left ventricular end-diastolic dimension and a 1.5–1.7-fold decrease in left ventricular wall thickness were observed in DT-treated TG, whereas these parameters were unchanged in mock-treated TG (Fig. 2, *C* and *D*) and DT- or mock-treated WT. Echocardiographic examination also demonstrated a 2.4-fold reduction in % FS in DT-treated TG. These results suggest that injection of DT induced deterioration of LV systolic function with chamber dilatation and ventricular wall thinning in TG. In contrast, no discernible phenotype was observed in TG in the absence of DT, and DT had no harmful effect on WT.

Hematoxylin-eosin staining of the histological sections of TG hearts 7 days after DT injection revealed degenerated cardiomyocytes surrounded by inflammatory cells (Fig. 3*A*). These pathological findings were not observed in WT with or without DT injection (data not shown). The infiltrating inflammatory cells were identified as macrophages by immunohistochemical analysis using anti-Mac-3 antibody (Fig. 3*B*). Histological sections with Masson's trichrome staining showed interstitial fibrosis in DT-treated TG hearts (Fig. 3*A*). Silver staining of the

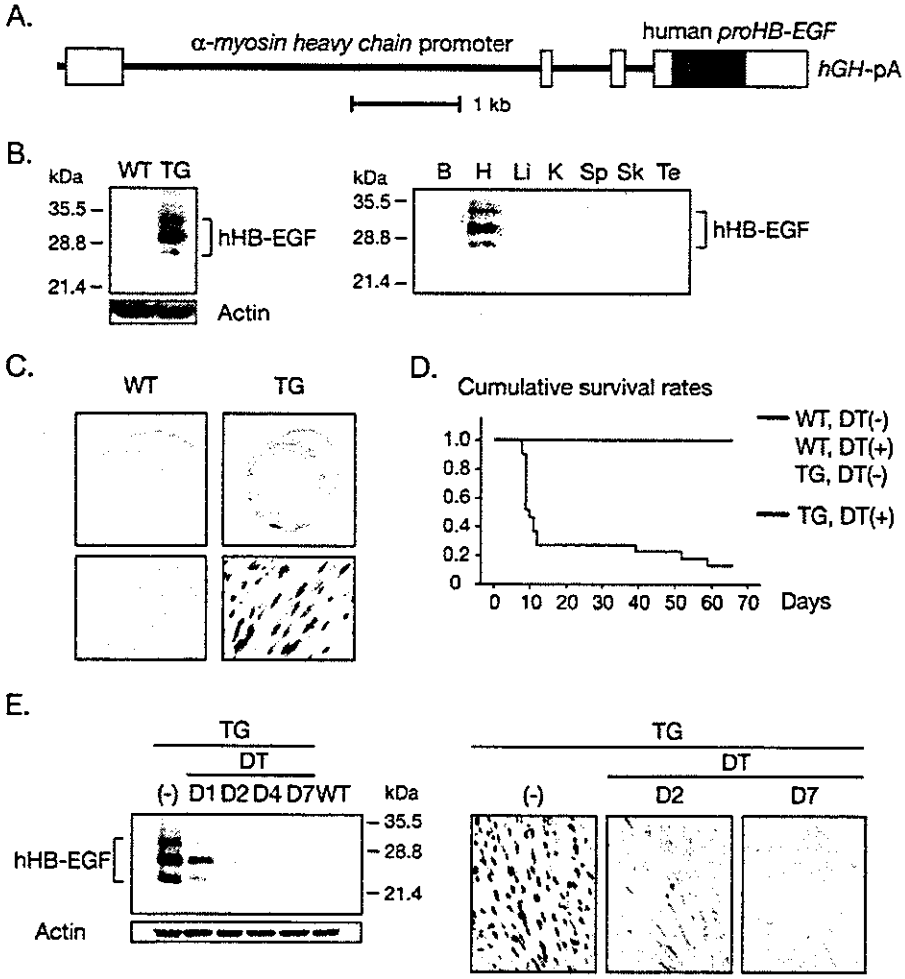

FIG. 1. **DT-induced myocardial cell ablation in transgenic mice expressing human *pro-HB-EGF*.** *A*, schematic representation of the transgene containing α-myosin heavy chain (*αMHC*) promoter, human *pro-HB-EGF* cDNA, and human growth hormone (*GH*) polyadenylation signal (*pA*). *B*, Western blot analysis using an antibody specific for human pro-HB-EGF revealed transgene expression in TG hearts (*left*). Expression of human pro-HB-EGF in TG was observed specifically in the hearts (*right*). *B*, brain; *H*, heart; *Li*, liver; *K*, kidney; *Sp*, spleen; *Sk*, skeletal muscle; *Te*, testis. *C*, *in situ* hybridization analysis using a riboprobe specific for human *pro-HB-EGF*. Transgene was expressed in a mosaic pattern, and cardiomyocytes expressing the transgene were 17.3 ± 6.0% of the total cardiomyocytes within TG hearts. *D*, Kaplan-Meier survival curves of control mice (WT treated with mock or DT and TG treated with mock, $n = 21$, respectively) and TG ($n = 21$) treated with intramuscular injection of DT. *E*, complete ablation of transgene-expressing cardiomyocytes following DT injection revealed by immunoblot (*left*) and *in situ* hybridization analysis. Expression of pro-HB-EGF was remarkably diminished on day 2 (*D2*) and was completely undetected on day 7 (*D7*).

sections of TG hearts on 14 days after DT injection revealed a 1.9-fold increase in cross-sectional areas of cardiomyocytes (Fig. 3*C*), indicating that the cardiomyocytes, which did not express the transgene and survived DT administration, underwent hypertrophic cell growth.

Alterations of Gene Expression in TG Presenting DT-induced Heart Failure—To characterize the molecular basis of heart failure caused by DT-induced myocardial cell ablation, we examined expression levels of several molecular markers. Expression of *BNP* was up-regulated 1 day after DT injection, and persistently elevated thereafter (Fig. 4). Increased expression of skeletal α-actin and decreased expression of *SERCA2* were evident 4 days after DT injection (Fig. 4). Up-regulation of natriuretic peptide genes and fetal cardiac genes including skeletal α-actin is one of the characteristic cellular responses observed during cardiac hypertrophy (32, 33). Especially, ventricular expression of *BNP* is induced promptly in response to volume expansion and pressure overload, and plasma BNP concentrations have proven to be valuable for diagnostic and prognostic assessment in patients with heart failure (34). In addition, down-regulation of *SERCA2* has been reported to be a sensitive marker for heart failure (35). Therefore, these patterns of cardiac gene expression indicated that DT-induced myocardial cell ablation burdened hemodynamic overload and progressed overt heart failure concomitantly with cardiac hypertrophy.

Consistent with the histological finding of infiltration by macrophages, an increase in expression of *MCP-1* was observed 1 day after DT injection, and expression levels of *MCP-1* were further increased until 4 days and declined on 7 days (Fig. 4). The expression levels of *TNF-α*, encoding an inflammatory cytokine produced by macrophages, changed in parallel with that of *MCP-1* (Fig. 4). Insomuch as symptomatic heart failure was evident 7 days after DT injection, stressed myocardium could be another source of *TNF-α* production at this period. Following up-regulation of inflammatory markers, expression levels of the collagen genes (*Col1a2* and *Col3a1*) were increased at 4 days after DT injection (Fig. 4). These temporal profiles of

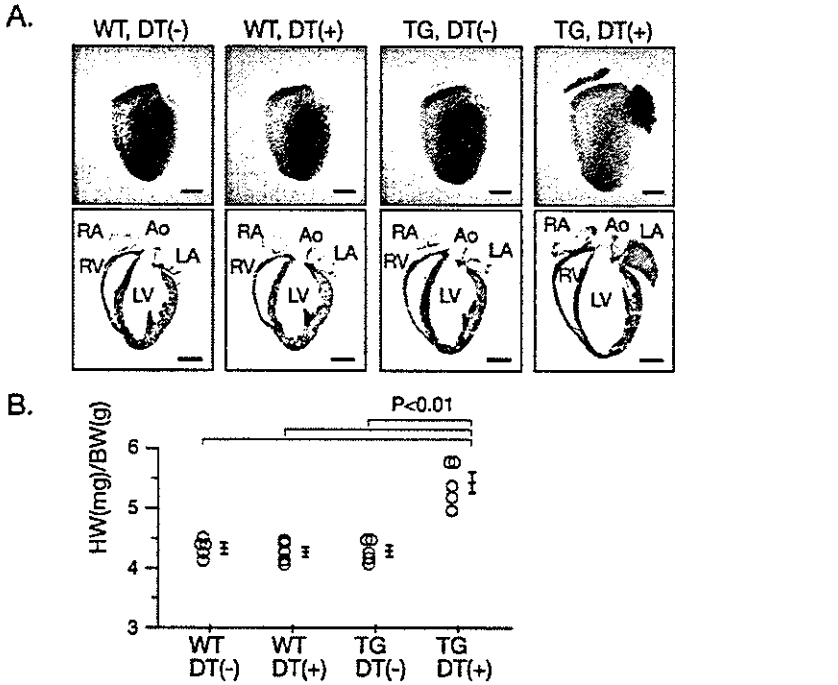

D.

	WT, DT(-)	WT, DT(+)	TG, DT(-)	TG, DT(+)
Number	10	10	10	10
Age (weeks)	10.7±0.4	10.6±0.5	11.5±0.3	10.9±0.3
BW(g)	24.0±1.7	24.1±1.2	24.8±0.4	24.3±1.3
HR (beats/min.)	261.0±15.9	258.9±18.8	256.3±18.4	252.3±18.0
LVDd (mm)	3.69±0.14	3.71±0.17	3.75±0.23	4.69±0.71
LVDs (mm)	2.05±0.13	2.11±0.20	2.08±0.27	3.81±0.46
FS (%)	44.2±4.7	43.2±4.9	47.4±3.5	19.4±3.0
IVSth (mm)	0.65±0.03	0.65±0.03	0.66±0.02	0.45±0.03
LVPWth (mm)	0.65±0.03	0.66±0.02	0.66±0.02	0.39±0.03

FIG. 2. **DT-induced cardiomyocyte loss caused heart failure in mice.** *A*, gross morphology of whole hearts (*upper rows*) and longitudinal sections (*lower rows*) of WT and TG 7 days after DT or mock injection. *Ao*, aorta; *LA*, left atrium; *LV*, left ventricle; *RA*, right atrium; *RV*, right ventricle. *Bar*, 2 mm. *B*, increase in heart to body weight ratios observed in TG 7 days after DT injection. *C*, representative M-mode echocardiograms. *IVS*, interventricular septum; *LVPW*, left ventricular posterior wall. *D*, echocardiographic measurements. *BW*, body weight; *FS*, fractional shortening; *HR*, heart rate; *IVSth*, interventricular thickness in end-diastole; *LVDd*, left ventricular diameter in end-diastole; *LVDs*, left ventricular diameter in end-systole; *LVPWth*, left ventricular posterior wall thickness in end-diastole.

gene expressions suggest that mobilization of macrophages are induced by up-regulated MCP-1 after the myocardial cell ablation, leading to cardiac fibrosis by enhanced production of inflammatory cytokines, and that inflammatory cytokines and cardiac remodeling might promote left ventricular dysfunction evoked by myocardial cell loss.

Myocardial Cell Death Induced by DT Is Not Primarily because of Apoptosis—To investigate the mechanisms of myocardial cell death in DT-treated TG hearts, we first performed a TUNEL assay. In the hearts of DT-treated TG, we could not detect any TUNEL-positive cardiomyocytes or inflammatory cells, whereas a marked increase in TUNEL-positive cells was detected in the spleen of mice treated with intraperitoneal administration of lipopolysaccharide as positive controls (Fig. 5*A*). Likewise, analysis of genomic DNA by agarose gel provided no evidence of DNA laddering in DT-treated TG hearts (Fig. 5*B*). We further examined activation of caspase 3 (Fig. 5*C*), changes in expression of proapoptotic and antiapoptotic Bcl2 family proteins (Fig. 5*D*), and cytochrome *c* release from mitochondria (Fig. 5*E*), but biochemi-

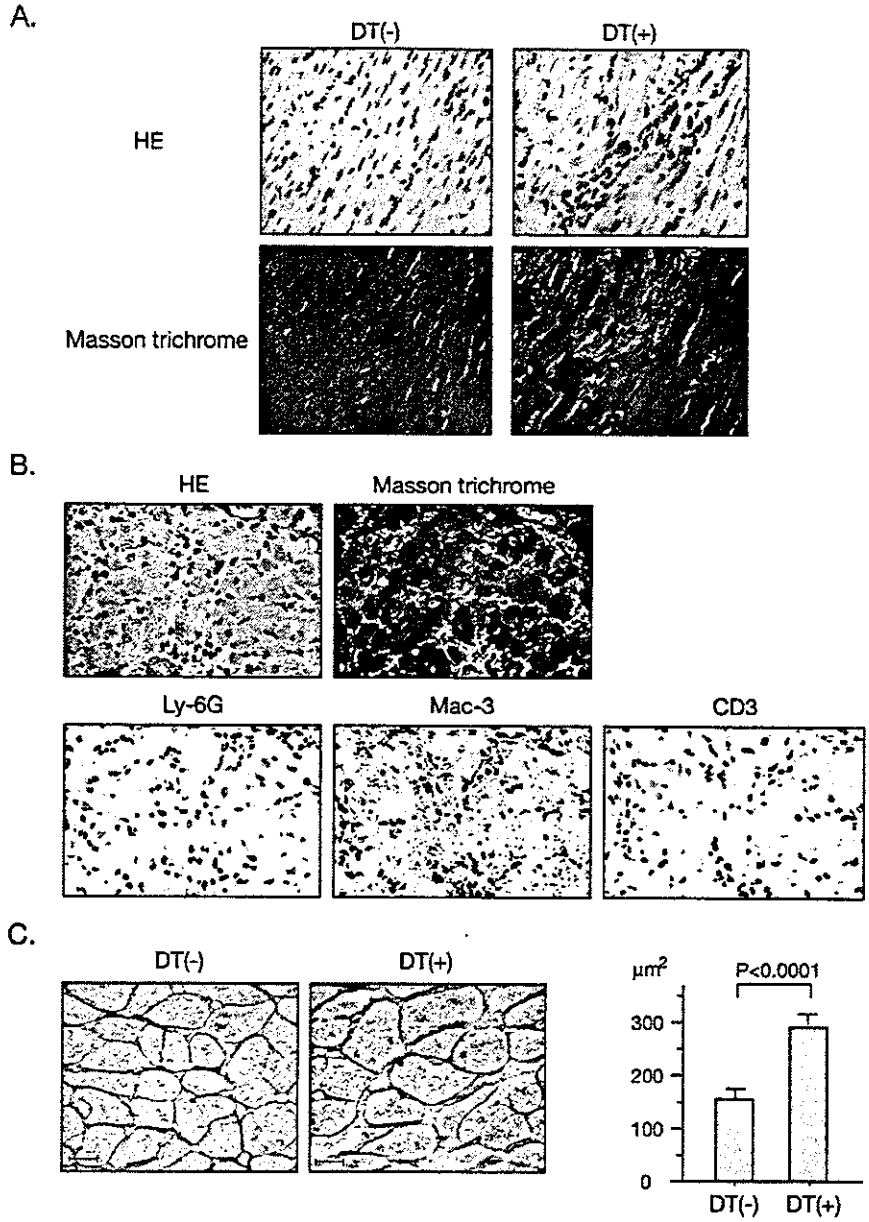

FIG. 3. **Histological analysis of the hearts after DT injection.** *A*, serial sections with hematoxylin-eosin (*HE*) staining revealed cardiomyocyte degeneration and infiltration of inflammatory cells 7 days after DT injection. Masson's trichrome staining showed interstitial fibrosis. *B*, infiltrating inflammatory cells were predominantly macrophages with positive staining for Mac-3 but not for Ly-6G nor CD3. *C*, silver staining of TG hearts 14 days after DT injection revealed an increase in the cross-sectional area of cardiomyocytes, indicating hypertrophic compensation of myocardial cells without transgene expression.

cal changes leading to typical apoptosis were not observed in DT-treated TG hearts.

Autophagy Is the Mechanism of Myocardial Cell Death in DT-induced Failing Hearts—ACD is a regulated process of caspase-independent programmed cell death, in which intracellular components are degradated by lysosomal or proteasomal proteases (21–23). Immunohistochemical analysis revealed positive staining for lysosomal protease cathepsin D, LAMP-1, and ubiquitin in cardiomyocytes of DT-treated TG hearts (Fig. 6*A*). It is notable that cathepsin D showed a diffuse cytosolic distribution, whereas LAMP-1 showed a granular localization. These results suggest an increase in formation of lysosomes and leakage of activated lysosomal enzymes into the cytosol. Recently, it has been reported that, in human failing hearts, ubiquitin accumulation in cardiomyocytes may be associated with up-regulation of ubiquitin-conjugating enzyme E2 (UBC2) and down-regulation of deubiquitinating enzymes such as UFD1 and isopeptidase T (6). However, Western blot analysis revealed that the amounts of the ubiquitin-activating enzyme E1, UBC2, ubiquitin-ligating enzyme E3 (E6-AP), and UFD1 were not unchanged in DT-treated TG hearts when compared with control hearts (Fig. 6*B*).

Electron microscopic analysis revealed abundant cytosolic vacuoles and segmented configuration of nuclei with lumpy con-

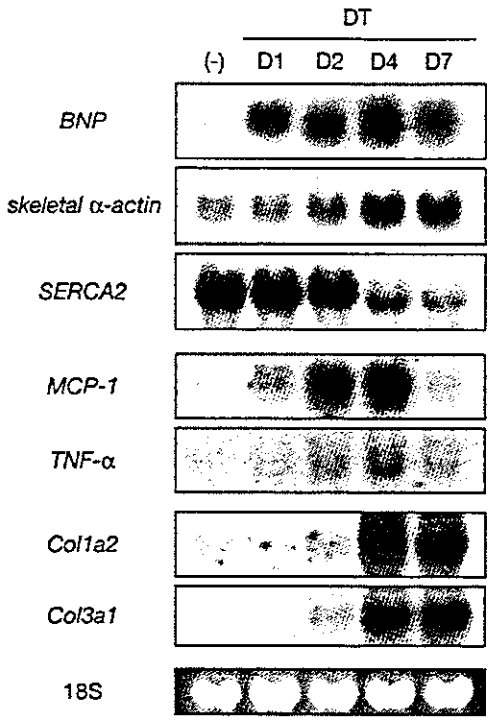

FIG. 4. **Alterations in gene expression after DT injection.** Temporal profiling of gene expression following administration of DT (5 mg/kg). Expression levels of cardiac genes, inflammatory cytokine genes, and collagen genes were examined by Northern blot analysis.

densation of chromatin in degenerated cardiomyocytes in TG hearts 3 days after DT injection (Fig. 7, *A* and *B*). However, nuclear fragmentation and crescent-shaped chromatin condensation at the nuclear periphery typical of apoptosis were not observed. In higher magnifications, cytosolic vacuoles containing lipid droplets with myelin figures and degenerated mitochondria (Fig. 7, *C* and *D*), suggested that these vacuoles are typical autophagosomes. In terminally degenerated cardiomyocytes, lysis of myofibrills and other intracellular organelles were prominent (Fig. 7*E*). These findings suggest that myocardial cell loss in DT-treated TG hearts is primarily because of ACD.

Autophagic degeneration has been implicated in human failing heart failure (3–7). We also found cardiomyocytes undergoing autophagic cell death in a biopsied specimen from a 43-year-old patient suffering from dilated cardiomyopathy. Similar to the electron micrographic findings in degenerated cardiomyocytes in our mouse model of heart failure, myofibrillar degeneration in association with cytosolic vacuoles and lipid droplets were observed in this biopsied specimen (Fig. 7*F*). The vacuoles were autophagosomes containing digested organelles. These findings are illustrative of the previously reported features characteristic of ACD in human heart failure. Therefore, degenerated cardiomyocytes in human dilated cardiomyopathy patients showed ultrastructural alterations similar to those in our mouse model of heart failure.

DISCUSSION

In this study, we generated a novel mouse model of heart failure, where cardiomyocyte loss through ACD is arbitrarily and specifically induced by intramuscular injection of DT. Recent technical progress in genetic manipulation and physiological measurements enabled us to produce several mouse models of heart failure (36). These models have improved our understanding of pathophysiology of heart failure and have been of great help for establishment and evaluation of new therapeutic approaches. Genetically engineered mice, in particular, expanded the list of gene products that are involved in generation or progression of heart failure, but they have specific limitations as animal models. For example, mice homozygous for muscle LIM protein (*MLP*) develop cardiomyopathy and heart failure, but the clinical courses of individual mice are divergent because the penetrance of phenotype is influenced by genetic backgrounds (37). About half of the *MLP*-deficient mice suffer from severe congestive heart failure and die during the second postnatal week, but the rest of the *MLP*-deficient mice survive to adulthood and are viable. Development of cardiomyopathy is also identified in tropomodulin-overexpressing transgenic mice (38). In this model, severe signs of heart failure are observed between 2 and 4 weeks after birth and most symptomatic mice die within a few days. The phenotypes of these model mice are primarily genotype-dependent, but are susceptible to the effects of genetic backgrounds. In addition, a difficulty in morphological and biochemical approach in studying a role of cardiomyocyte death in heart failure arises from the low occurrence of cell death in these models (2). In our mouse model of heart failure, cardiomyocytes expressing the DT receptor are selectively and simultaneously damaged by administration of DT, and this advantageous feature not only makes it possible to induce symptomatic heart failure arbitrarily but also provides insights into the roles of cell death in heart failure.

Our model appears conceptually similar to the one reported in the earlier work (39), in which DT-A expression is regulated by a tetracycline-responsive promoter. In that model, induction of DT-A in the hearts resulted in congestive heart failure as well. However, a leaky induction is occasionally observed in this tetracycline-inducible system, and subtle expression of DT-A might have nonspecific and undesirable effects, insomuch as the toxicity of DT-A is extremely high (17). In our model, the DT receptor, not injurious in the absence of DT, was expressed in the hearts, and myocardial cell ablation was specifically and ideally achieved.

Temporal histological analysis and profiling of gene expression revealed a series of cellular events that finally evoked heart failure (Figs. 3 and 4). Transgene expression was dramatically reduced in a few days after DT injection (Fig. 1*E*), suggesting that cardiomyocyte death occurs during that period. Following cardiomyocyte death, inflammatory cells infiltrated and produced inflammatory cytokines. Around 7 days, hemodynamic deterioration with apparent cardiac remodeling induced symptomatic heart failure. These findings strongly suggest that myocardial cell death causes symptomatic heart failure. In addition, our model allowed quantitative analysis of cardiomyocyte death. *In situ* hybridization analysis revealed that expression of the transgene was scattered diffusely and observed in 17.3 ± 6.0% of cardiomyocytes in TG hearts. Because there was no cardiomyocyte expressing the transgene on day 7 after DT injection, all of the transgene-expressing cells (~17% of cardiomyocytes) might be dead. These results suggest that loss of this population is sufficient to produce symptomatic heart failure, and this estimation is consistent with the notion that a diffuse loss of 10–20% of cardiomyocytes accounts for cardiac failure, whereas equivalent cardiac failure is produced by a segmental loss of 40–50% of cardiomyocytes after coronary artery occlusion (40).

Electron microscopic analysis revealed that, in our mouse model, damaged cardiomyocytes showed abundant cytoplasmic autophagosomes and chromatin condensation with more complex and lumpier shapes than in apoptosis, both of which are characteristic of ACD (Fig. 7). ACD is defined as a regulated pathway of cytoplasmic degradation executed by lysosomal and

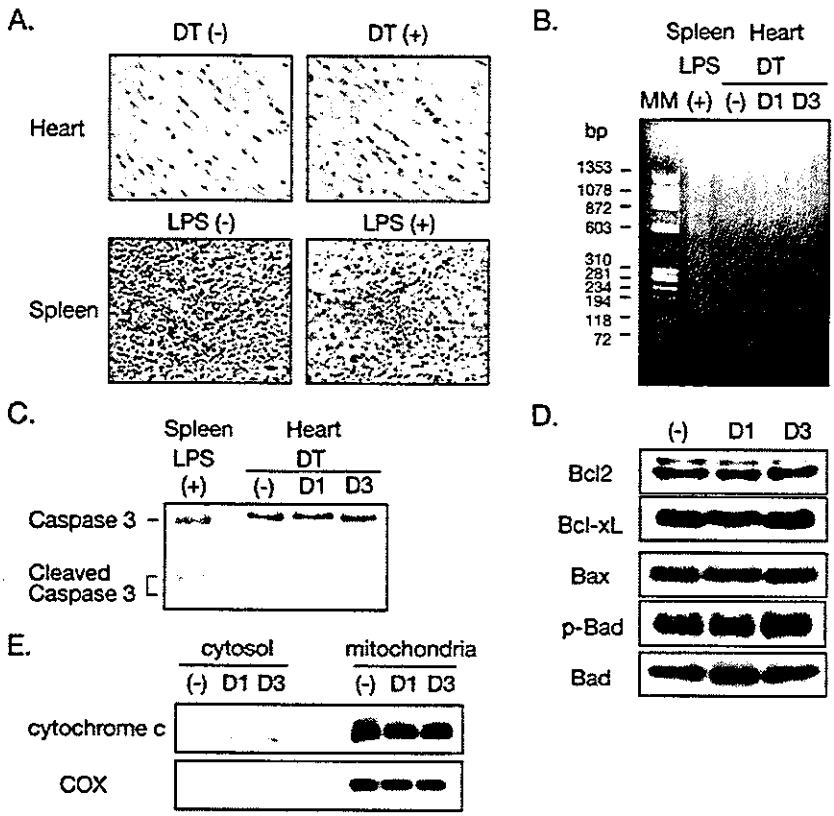

FIG. 5. **DT-induced myocardial cell death is not mediated by apoptosis, but by autophagy.** *A* and *B*, TUNEL method (*A*) and electrophoresis of genomic DNA by agarose gel (*B*) showed no evidence of DNA fragmentation in TG hearts 3 days after DT injection. Spleens from mice with lipopolysaccharide-induced sepsis were used as a positive control. *C–E*, immunoblot analysis showing no evidence of activation of caspase 3 (*C*), changes in expressions of Bcl2 family proteins (*D*) and cytochrome *c* release from mitochondria (*E*) in DT-treated TG hearts. *COX*, cytochrome *c* oxidase subunit IV. *D*, day. *LPS*, lipopolysaccharide.

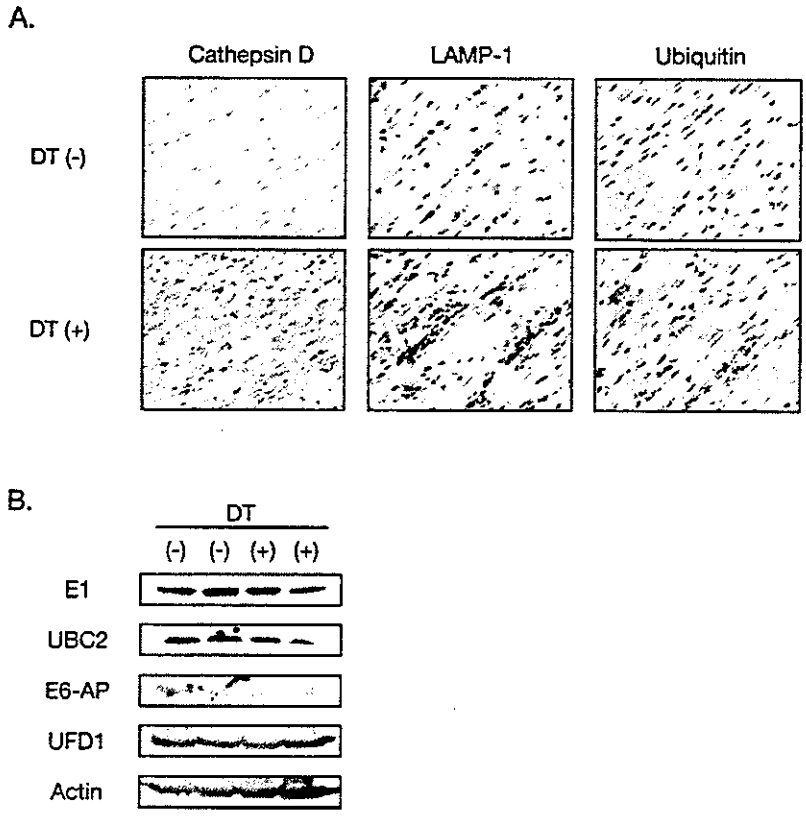

FIG. 6. **DT-induced myocardial cell death is mediated by autophagy.** *A*, immunohistochemistry showing cardiomyocytes were positively stained for cathepsin D, LAMP-1, and ubiquitin in TG hearts 3 days after DT injection. *B*, immunoblot analysis showing unchanged expression levels of the ubiquitin-activating enzyme E1, ubiquitin-conjugating enzyme E2 (*UBC2*), ubiquitin-ligating enzyme E3 (*E6-AP*), and deubiquitinating enzyme UFD1.

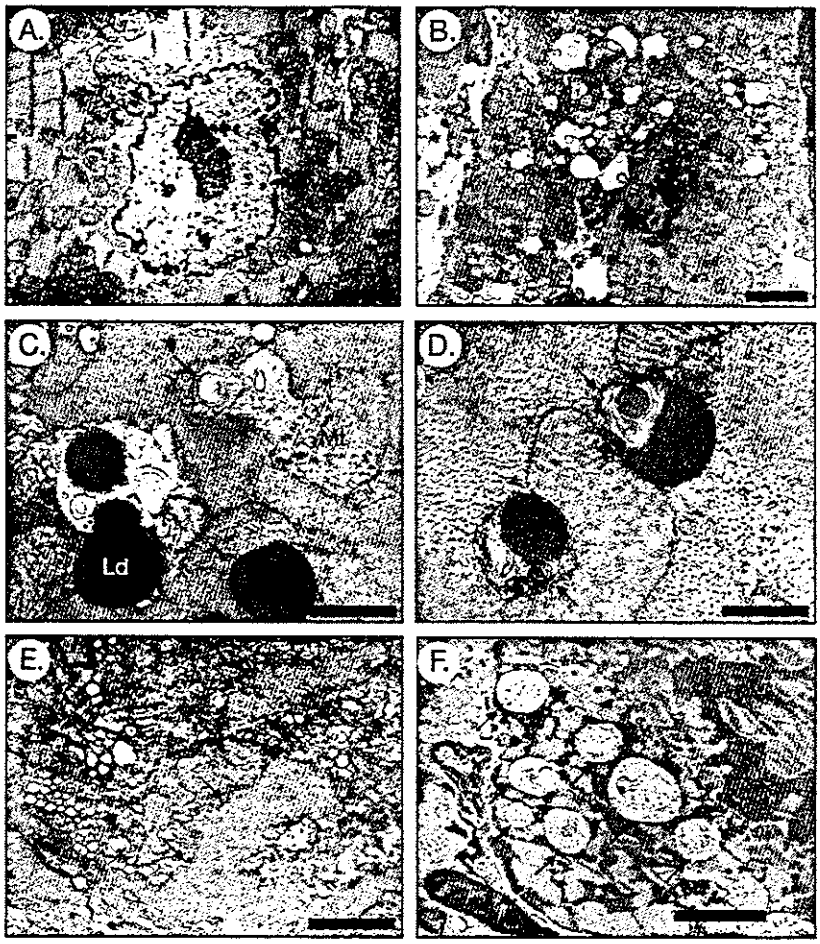

FIG. 7. **Electron microscopic analysis of the hearts after DT injection.** Electron microscopic analysis before (*A*) and after DT injection (*B–E*). In cardiomyocytes of DT-treated TG hearts, nuclear morphological changes associated with lumpy chromatin condensation were observed (*arrow* in *B*). Abundant vacuoles of various sizes in the cytoplasm (*B*) were typical autophagosomes containing degenerating lipid droplets and mitochondria (*C* and *D*). *Arrows* (in *C* and *D*) indicate myelin figures. Myofibrillar lysis (*arrows*) was observed in cardiomyocytes undergoing autophagic cell death (*E*). Electron microscopic analysis of biopsied myocardium from a patient with dilated cardiomyopathy (*F*) revealed cardiomyocytes containing many autophagosomes with degenerating mitochondria (*arrows*). *Ld*, lipid droplet; *Mt*, mitochondria. *Bars*, 2 μm (*A* and *B*), 1 μm (*C* and *E*), 0.5 μm (*D*), and 5 μm (*F*).

proteasomal proteases (21–23, 41). Consistently, elevated expressions of cathepsin D and ubiquitin were recognized in DT-treated TG cardiomyocytes (Fig. 6*A*). In contrast, biochemical signals inducing apoptosis were not activated. ACD often occurs in large, cytoplasmic-rich, and post-mitotic cells, and has been implicated in several human diseases (19, 21–23, 41). For example, ACD is associated with neurodegenerative diseases such as Parkinson's disease (42), Huntington's disease (43), and Alzheimer's disease (44). Degenerated cardiomyocytes displaying morphological features characteristic of ACD have recently been reported to exist in the failing hearts of patients with dilated cardiomyopathy, valvular heart diseases, congenital heart diseases, and hypertensive heart diseases (Fig. 7*F*) (3–7). A recent paper demonstrated that cardiomyocyte apoptosis of rare occurrence comparable with that observed in human failing hearts were sufficient to cause lethal cardiomyopathy in transgenic mice with a ligand-induced caspase-8 activation in the hearts (45). It is noteworthy that autophagic cardiomyocyte death has been reported to be detectable more frequently than apoptosis or oncosis in failing or hemodynamically overloaded human hearts (3, 6, 7), although the frequency of the each form of cell death may be influenced by disease stages and backgrounds (*e.g.* age, etiology, clinical feature, and treatment) of the examined samples (2).

Recent studies have indicated a significant role of lysosomal cysteine and aspartic protease cathepsins in execution of ACD (21, 46). PC12 cells cultured in a serum-deprived condition showed morphological features characteristic of ACD with an increase in proteolytic activity of cathepsin D (46), and forced expression of cathepsin D in PC12-induced rapid cell death, indicating a regulatory role of cathepsin D in ACD. Expression of cathepsin D was increased in DT-treated TG hearts (Fig. 6*A*). In damaged cardiomyocytes, translocation of cathepsin D from lysosomes to the cytosol was evident, which is indicative of enhanced proteolytic activity (47). Cathepsin D has been reported to be activated in human failing hearts (5) and also to be a positive mediator of apoptotic cell death (22, 47). Further experiments are required to clarify whether cathepsin D is involved in execution of myocardial ACD in the pathogenesis of heart failure and how cathepsin D regulates these modes of cell death differentially.

According to the recent studies, ubiquitin-dependent protein degradation is linked to autophagy (48). Accumulation of ubiquitin in cardiomyocytes was observed in DT-treated TG hearts (Fig. 6*A*) as well as in human failing hearts (4, 6, 7). Kostin *et al.* (6) demonstrated a functional defect in the ubiquitin/proteasome pathway together with ubiquitin accumulation in human failing hearts, and speculated that an excess of ubiquitinated proteins might activate autophagic protein degradation. The precise molecular mechanisms of how ubiquitin accumulation enhances autophagy remain unknown, although ubiquitination is postulated to be required for maturation of autophagosomes (48). Unlike human failing hearts (6), the amounts of UBC2 and UFD1 were unchanged in the hearts of our model mice (Fig. 6*B*). Protein ubiquitination and deubiquitination are mediated by a large number of enzymes (49), and it is an important issue to be

addressed in the future how ubiquitin is accumulated in cardiomyocytes undergoing autophagic cell death.

Diphtheria is a communicable disease affecting the upper respiratory tract and occasionally the skin as primary infection (50). However, remote organs such as heart or peripheral nerves are often damaged when DT is absorbed into the systemic circulation. Although diphtheria infection has been rarely encountered in developed countries because of the high rates of vaccination after the mid 1960s, several sporadic outbreaks occurred, for example, in the former Union of Soviet Socialist Republics in 1990s (50). Myocardial involvement is a major complication that determines the prognosis, but the pathophysiology associated with diphtheritic cardiomyopathy remains largely unknown. Histological analysis of the postmortal heart of a diphtheria patient revealed hyaline degeneration of myocardium and infiltration of mononuclear cells, and cytosolic lipid droplets and clumped chromatin granules were observed by electron microscopic examination (51). Although vacuoles of autophagosomes were not described in this paper, these findings were similar to those observed in our mouse model. Interestingly, cardiomyocyte loss through ACD associated with a decrease in protein synthesis was also observed in anthracycline-induced cardiomyopathy (52). Therefore, autophagic cardiomyocyte death evoked by a decrease in protein synthesis might not be confined to diphtheritic cardiomyopathy, but a more generalized phenomenon that occurs during progression of heart failure arising from miscellaneous etiologies. In this regard, our model of experimentally induced heart failure will be useful to elucidate molecular mechanisms underlying structural and functional changes associated with ACD in heart failure.

Acknowledgments—We thank R. Kobayashi, E. Fujita, and M. Iida for excellent technical assistance. We are grateful to Dr. A. Ullrich (Max-Planck-Institute of Biochemistry, Martinsried, Germany) and Dr. J. Robbins (Children's Hospital, Cincinnati, OH) for providing cDNAs.

REFERENCES

1. Nadal, G. B., Kajstura, J., Leri, A., and Anversa, P. (2003) *Circ. Res.* **92,** 139–150
2. Kang, P. M., and Izumo, S. (2000) *Circ. Res.* **86,** 1107–1113
3. Yamamoto, S., Sawada, K., Shimomura, H., Kawamura, K., and James, T. N. (2000) *J. Mol. Cell Cardiol.* **32,** 161–175
4. Knaapen, M. W., Davies, M. J., De, B. M., Haven, A. J., Martinet, W., and Kockx, M. M. (2001) *Cardiovasc. Res.* **51,** 304–312
5. Shimomura, H., Terasaki, F., Hayashi, T., Kitaura, Y., Isomura, T., and Suma, H. (2001) *Jpn. Circ. J.* **65,** 965–968
6. Kostin, S., Pool, L., Elsasser, A., Hein, S., Drexler, H. C., Arnon, E., Hayakawa, Y., Zimmermann, R., Bauer, E., Klovekorn, W. P., and Schaper, J. (2003) *Circ. Res.* **92,** 715–724
7. Hein, S., Arnon, E., Kostin, S., Schonburg, M., Elsasser, A., Polyakova, V., Bauer, E. P., Klovekorn, W. P., and Schaper, J. (2003) *Circulation* **107,** 984–991
8. Mann, D. L. (1999) *Circulation* **100,** 999–1008
9. Schaper, J., Elsasser, A., and Kostin, S. (1999) *Circ. Res.* **85,** 867–869
10. Anversa, P. (2000) *Circ. Res.* **86,** 121–124
11. Pappenheimer, A. J. (1977) *Annu. Rev. Biochem.* **46,** 69–94
12. Falnes, P. O., and Sandvig, K. (2000) *Curr. Opin. Cell Biol.* **12,** 407–413
13. Van Ness, B. G., Howard, J. B., and Bodley, J. W. (1980) *J. Biol. Chem.* **255,** 10710–10716
14. Higashiyama, S., Abraham, J. A., Miller, J., Fiddes, J. C., and Klagsbrun, M. (1991) *Science* **251,** 936–939
15. Naglich, J. G., Metherall, J. E., Russell, D. W., and Eidels, L. (1992) *Cell* **69,** 1051–1061
16. Mitamura, T., Umata, T., Nakano, F., Shishido, Y., Toyoda, T., Itai, A., Kimura, H., and Mekada, E. (1997) *J. Biol. Chem.* **272,** 27084–27090
17. Saito, M., Iwawaki, T., Taya, C., Yonekawa, H., Noda, M., Inui, Y., Mekada, E., Kimata, Y., Tsuru, A., and Kohno, K. (2001) *Nat. Biotechnol.* **19,** 746–750
18. Kim, J., and Klionsky, D. J. (2000) *Annu. Rev. Biochem.* **69,** 303–342
19. Klionsky, D. J., and Emr, S. D. (2000) *Science* **290,** 1717–1721
20. Ohsumi, Y. (2001) *Nat. Rev. Mol. Cell. Biol.* **2,** 211–216
21. Bursch, W. (2001) *Cell Death Differ.* **8,** 569–581
22. Leist, M., and Jaattela, M. (2001) *Nat. Rev. Mol. Cell. Biol.* **2,** 589–598
23. Lockshin, R. A., and Zakeri, Z. (2002) *Curr. Opin. Cell Biol.* **14,** 727–733
24. Takano, H., Nagai, T., Asakawa, M., Toyozaki, T., Oka, T., Komuro, I., Saito, T., and Masuda, Y. (2000) *Circ. Res.* **87,** 596–602
25. Asakawa, M., Takano, H., Nagai, T., Uozumi, H., Hasegawa, H., Kubota, N., Saito, T., Masuda, Y., Kadowaki, T., and Komuro, I. (2002) *Circulation* **105,** 1240–1246
26. Toko, H., Zhu, W., Takimoto, E., Shiojima, I., Hiroi, Y., Zou, Y., Oka, T., Akazawa, H., Mizukami, M., Sakamoto, M., Terasaki, F., Kitaura, Y., Takano, H., Nagai, T., Nagai, R., and Komuro, I. (2002) *J. Biol. Chem.* **277,** 24735–24743
27. Akazawa, H., Komuro, I., Sugitani, Y., Yazaki, Y., Nagai, R., and Noda, T. (2000) *Genes Cells* **5,** 499–513
28. Vander, H. M., Chandel, N. S., Williamson, E. K., Schumacker, P. T., and Thompson, C. B. (1997) *Cell* **91,** 627–637
29. Saito, S., Hiroi, Y., Zou, Y., Aikawa, R., Toko, H., Shibasaki, F., Yazaki, Y., Nagai, R., and Komuro, I. (2000) *J. Biol. Chem.* **275,** 34528–34533
30. Chau, B. N., Borges, H. L., Chen, T. T., Masselli, A., Hunton, I. C., and Wang, J. Y. (2002) *Nat. Cell Biol.* **4,** 757–765
31. Komazaki, S., Ito, K., Takeshima, H., and Nakamura, H. (2002) *FEBS Lett.* **524,** 225–229
32. Komuro, I., and Yazaki, Y. (1993) *Annu. Rev. Physiol.* **55,** 55–75
33. Sadoshima, J., and Izumo, S. (1997) *Annu. Rev. Physiol.* **59,** 551–571
34. de Lemos, J. A., McGuire, D. K., and Drazner, M. H. (2003) *Lancet* **362,** 316–322
35. Mercadier, J. J., Lompre, A. M., Duc, P., Boheler, K. R., Fraysse, J. B., Wisnewsky, C., Allen, P. D., Komajda, M., and Schwartz, K. (1990) *J. Clin. Investig.* **85,** 305–309
36. Elsner, D., and Riegger, G. A. (1995) *Curr. Opin. Cardiol.* **10,** 253–259
37. Arber, S., Hunter, J. J., Ross, J. J., Hongo, M., Sansig, G., Borg, J., Perriard, J. C., Chien, K. R., and Caroni, P. (1997) *Cell* **88,** 393–403
38. Sussman, M. A., Welch, S., Cambon, N., Klevitsky, R., Hewett, T. E., Price, R., Witt, S. A., and Kimball, T. R. (1998) *J. Clin. Investig.* **101,** 51–61
39. Lee, P., Morley, G., Huang, Q., Fischer, A., Seiler, S., Horner, J. W., Factor, S., Vaidya, D., Jalife, J., and Fishman, G. I. (1998) *Proc. Natl. Acad. Sci. U. S. A.* **95,** 11371–11376
40. Anversa, P., Zhang, X., Li, P., and Capasso, J. (1992) *J. Clin. Investig.* **89,** 618–629
41. Lockshin, R. A., Osborne, B., and Zakeri, Z. (2000) *Cell Death Differ.* **7,** 2–7
42. Anglade, P., Vyas, S., Javoy-Agid, F., Herrero, M. T., Michel, P. P., Marquez, J., Mouatt-Prigent, A., Ruberg, M., Hirsch, E. C., and Agid, Y. (1997) *Histol. Histopathol.* **12,** 25–31
43. Kegel, K. B., Kim, M., Sapp, E., McIntyre, C., Castano, J. G., Aronin, N., and DiFiglia, M. (2000) *J. Neurosci.* **20,** 7268–7278
44. Cataldo, A. M., Hamilton, D. J., Barnett, J. L., Paskevich, P. A., and Nixon, R. A. (1996) *J. Neurosci.* **16,** 186–199
45. Wencker, D., Chandra, M., Nguyen, K., Miao, W., Garantziotis, S., Factor, S. M., Shirani, J., Armstrong, R. C., and Kitsis, R. N. (2003) *J. Clin. Investig.* **111,** 1497–1504
46. Uchiyama, Y. (2001) *Arch. Histol. Cytol.* **64,** 233–246
47. Roberg, K., and Ollinger, K. (1998) *Am. J. Pathol.* **152,** 1151–1156
48. Blommaart, E. F., Luiken, J. J., and Meijer, A. J. (1997) *Histochem. J.* **29,** 365–385
49. Pickart, C. M. (2004) *Cell* **116,** 181–190
50. Hadfield, T. L., McEvoy, P., Polotsky, Y., Tzinserling, V. A., and Yakovlev, A. A. (2000) *J. Infect. Dis.* **181,** Suppl. 1, S116–S120
51. Burch, G. E., Sun, S. C., Sohal, R. S., Chu, K. C., and Colcolough, H. L. (1968) *Am. J. Cardiol.* **21,** 261–268
52. Semenov, D. E., Lushnikova, E. L., and Nepomnyashchikh, L. M. (2001) *Bull. Exp. Biol. Med.* **131,** 505–510

Vasorin, a transforming growth factor β-binding protein expressed in vascular smooth muscle cells, modulates the arterial response to injury *in vivo*

Yuichi Ikeda*†‡, Yasushi Imai†, Hidetoshi Kumagai*§, Tetsuya Nosaka*, Yoshihiro Morikawa¶, Tomoko Hisaoka¶, Ichiro Manabe†, Koji Maemura†, Takashi Nakaoka‖, Takeshi Imamura**, Kohei Miyazono††, Issei Komuro‡‡, Ryozo Nagai†, and Toshio Kitamura*‡§§

Divisions of *Hematopoietic Factors and §§Cellular Therapy and ‖Department of Advanced Medicine, Institute of Medical Science, University of Tokyo, Tokyo 108-8639, Japan; Departments of †Cardiovascular Medicine and ††Molecular Pathology, Graduate School of Medicine, University of Tokyo, Tokyo 113-8655, Japan; §Takada Research Laboratories, Chugai Pharmaceutical Company, Limited, Tokyo 171-8545, Japan; ¶Department of Anatomy and Neurobiology, Wakayama Medical School, Wakayama 641-8509, Japan; **Department of Biochemistry, Cancer Institute of the Japanese Foundation for Cancer Research, Tokyo 170-8455, Japan; and ‡‡Department of Cardiovascular Science and Medicine, Graduate School of Medicine, Chiba University, Chiba 260-8670, Japan

Communicated by Masashi Yanagisawa, University of Texas Southwestern Medical Center, Dallas, TX, June 9, 2004 (received for review February 25, 2004)

Growth factors, cell-surface receptors, adhesion molecules, and extracellular matrix proteins play critical roles in vascular pathophysiology by affecting growth, migration, differentiation, and survival of vascular cells. In a search for secreted and cell-surface molecules expressed in the cardiovascular system, by using a retrovirus-mediated signal sequence trap method, we isolated a cell-surface protein named vasorin. Vasorin is a typical type I membrane protein, containing tandem arrays of a characteristic leucine-rich repeat motif, an epidermal growth factor-like motif, and a fibronectin type III-like motif at the extracellular domain. Expression analyses demonstrated that vasorin is predominantly expressed in vascular smooth muscle cells, and that its expression is developmentally regulated. To clarify biological functions of vasorin, we searched for its binding partners and found that vasorin directly binds to transforming growth factor (TGF)-β and attenuates TGF-β signaling *in vitro*. Vasorin expression was down-regulated during vessel repair after arterial injury, and reversal of vasorin down-regulation, by using adenovirus-mediated *in vivo* gene transfer, significantly diminished injury-induced vascular lesion formation, at least in part, by inhibiting TGF-β signaling *in vivo*. These results suggest that down-regulation of vasorin expression contributes to neointimal formation after vascular injury and that vasorin modulates cellular responses to pathological stimuli in the vessel wall. Thus, vasorin is a potential therapeutic target for vascular fibroproliferative disorders.

Vascular smooth muscle cells (VSMCs), the major cell type in the vessel wall, show a spectrum of phenotypes, depending on environmental cues. Various injurious stimuli provoke the proliferation of differentiated medial VSMCs, which migrate to the intima and produce extracellular matrix proteins, resulting in the narrowing of the vascular lumen. These processes, called VSMC phenotypic modulation, play a key role in development of atherosclerotic diseases, such as postangioplasty restenosis, vein graft disease, and transplant vasculopathy. Whereas tremendous progress has been made in identifying growth factors and transcription factors that regulate the vascular response to injury, much information is lacking regarding cell-surface molecules that are involved in the pathogenesis of vascular fibroproliferative disorders. The signal sequence trap (SST) is a strategy to identify cDNAs containing signal sequence that encode secreted and type I membrane proteins (1, 2). We recently developed a refined SST system based on retrovirus-mediated expression screening (SST-REX) (3). In a search for secreted and cell-surface molecules expressed in the cardiovascular system, by using SST-REX, we identified a TGF-β binding protein, vasorin. Vasorin is predominantly expressed in VSMCs and modulates the vascular response to injury, at least in part, by attenuating TGF-β signaling *in vivo*. Here, we describe the molecular and functional characteristics of vasorin.

Methods

Cells and Reagents. A murine pro-B cell line Ba/F3 was maintained in RPMI medium 1640 containing 10% FCS and 2 ng/ml murine IL-3 (R & D Systems). Chinese hamster ovary (CHO) cells were grown in DMEM supplemented with 5% FCS and 1% nonessential amino acids (Invitrogen). Stable transfectants were established by the retrovirus expression system, by using a bicistronic retroviral vector pMX-IRES-EGFP as reported (4). Rat aortic VSMCs, prepared from 8-week-old Wistar rats by using the explant method (5), were grown in DMEM supplemented with 10% FCS. Primary antibodies used in this study were anti-Flag monoclonal antibody (M2, Sigma), anti-Smad2/3 monoclonal antibody (BD Transduction Laboratories), anti-phospho-Smad2 polyclonal antibody (Upstate, Charlottesville, VA), and anti-rat CD45 monoclonal antibody (BD Pharmingen).

Screening of a Human Heart cDNA Library by SST-REX and Cloning of the Full-Length cDNA Encoding *Vasorin*. A human heart cDNA library was screened by SST-REX as described (3). Briefly, cDNA was synthesized from poly(A)$^+$ RNA of human hearts (Clontech), by using the SuperScript Choice system (Invitrogen). The synthesized cDNA was separated based on size, and fractions >600 bp were inserted into *Bst*XI sites of the pMX-SST vector, by using *Bst*XI adapters (Invitrogen). Ba/F3 cells were infected with high-titer retroviruses expressing the human heart cDNA library, and the integrated cDNA fragments were isolated from factor-independent Ba/F3 clones by genomic PCR. All cDNA fragments were sequenced and analyzed. Subsequently, a human heart cDNA library in the pME18S vector was screened by using the ^{32}P-labeled cDNA fragment of a clone so as to isolate the entire coding region.

RNA, Protein, and Histological Analyses. Northern blot, *in situ* hybridization, semiquantitative RT-PCR, immunoprecipitation, Western blot, and histological analyses were done as described

Abbreviations: VSMC, vascular smooth muscle cell; TGF, transforming growth factor; EGF, epidermal growth factor; SST, signal sequence trap; SST-REX, retrovirus-mediated SST; CHO, Chinese hamster ovary; RA, retinoic acid; E*n*, embryonic day *n*; LRR, leucine-rich repeat; Ad, adenovirus; Ad-vasorin, Ads expressing vasorin-Flag; PDGF, platelet-derived growth factor.

Data deposition: The sequence reported in this paper has been deposited in the GenBank database (accession no. AY166584).

*To whom correspondence may be addressed at: 4-6-1, Shirokanedai, Minato-ku, Tokyo 108-8639, Japan. E-mail: yikeda-tky@umin.ac.jp or kitamura@ims.u-tokyo.ac.jp.

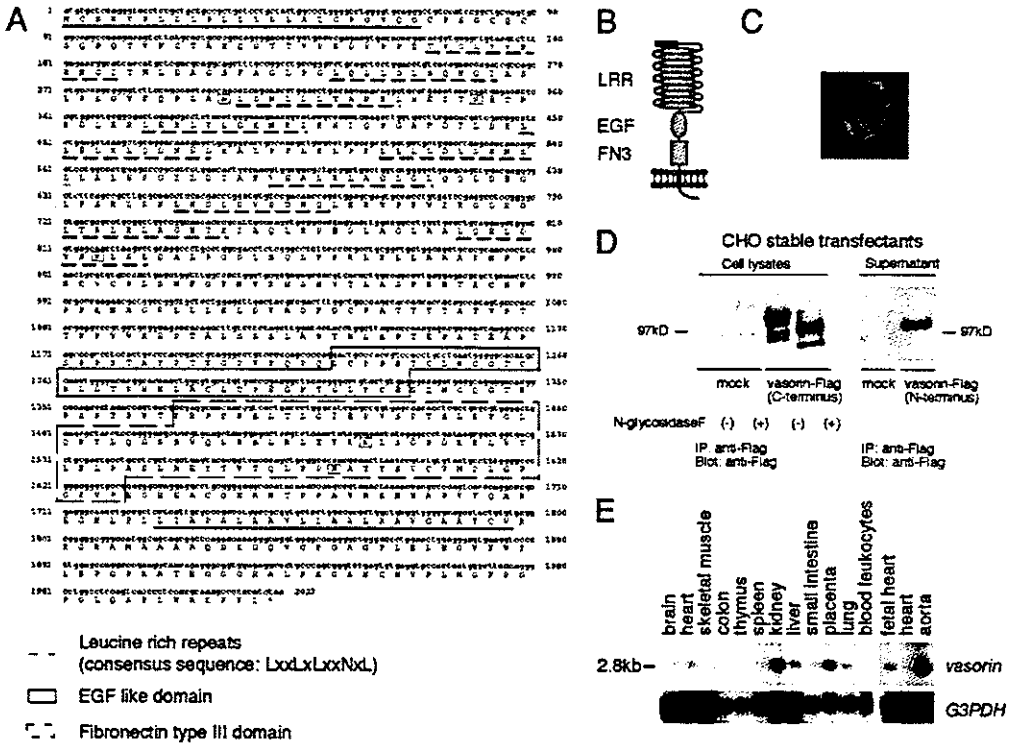

Fig. 1. Vasorin, an identified cell-surface protein. (*A*) Deduced amino acid sequence of human vasorin. The putative signal peptide (underlined), the LRRs (dotted underlines), the EGF motif (boxed), the fibronectin type III motif (dotted boxes), the transmembrane sequence (underlined), and five putative N-glycosylation sites (boxed) are indicated. (*B*) Structural model of vasorin. (*C*) Immunofluorescence analysis of subcellular localization of vasorin. Vasorin was expressed on the cell surface. (*D*) Cell lysates and supernatants of CHO cells stably expressing vasorin-Flag were subjected to immunoprecipitation and Western blot analysis by using an anti-Flag antibody. An ≈110-kDa protein for membrane-bound vasorin with C-terminal tag and a ≈100-kDa protein for soluble vasorin with N-terminal tag were detected under reducing conditions. N-glycosidase F treatment revealed that vasorin is N-glycosylated. (*E*) Northern blot analysis of adult human tissues. A single intense 2.8-kb band was detected and the strongest expression was observed in the aorta.

in *Supporting Text*, which is published as supporting information on the PNAS web site.

Production of the Recombinant Vasorin-Fc Chimera Protein. The bicistronic retroviral vector containing the *vasorin*-Fc chimera, pMX-*vasorin*-Fc chimera-IRES-EGFP, was constructed by inserting the cDNA for the whole-extracellular domain of human *vasorin* and the cDNA for the human Ig Fc region. CHO cells stably expressing the *vasorin*-Fc chimera were expanded in the medium supplemented with 2.5% Ultralow IgG FCS (Invitrogen) and 1% nonessential amino acids (Invitrogen). Secreted recombinant vasorin-Fc chimera protein was purified from the media of infected CHO cells by using Hitrap protein A columns (Amersham Biosciences).

Surface Plasmon Resonance Analysis. The BIAcoreTM2000 system (BIAcore, Uppsala) was used to characterize the interaction and to determine binding characteristics between the recombinant vasorin-Fc and TGF-β1, according to the manufacturer's instructions. To immobilize TGF-β1 on CM5 sensor chips, recombinant human TGF-β1 (R & D Systems) solution in 10 mM acetic acid (pH 4.0) was injected until the desired amount of coupled TGF-β1 was achieved, by using the standard amine-coupling procedure. All experiments were performed at room temperature by using the KINJECT command at a flow rate of 20 μl/min. Responses obtained on control chips were subtracted from those obtained on chips coupled with TGF-β1. Sensorgrams were analyzed by using BIAEVALUATION software (version 3.0).

Transient Transfection and Reporter Assay. CHO stable transfectants were transiently transfected with TGF-β1-responsive luciferase reporter plasmid (p3TP-lux) together with a β-galactosidase reporter plasmid driven by Rous sarcoma virus-LTR as an internal control, by using FuGENE6 (Roche Diagnostics, Roskilde, Denmark). After 24 h, the cells were stimulated for 24 h by adding TGF-β1 (R & D Systems) and were then assayed for luciferase and β-galactosidase activities. Experiments were performed several times and representative data are shown.

Rat Arterial Balloon-Injury Model. Adult rats (weighing 400–450 g) were anesthetized with chloral hydrate (370 mg/kg i.p.). Balloon denudation of the left common carotid artery was done by using a 2F Fogarty catheter (Baxter Edwards Healthcare, Irvine, CA), as described (6). The right common carotid artery served as a control. Rats were killed 3 or 14 days after injury, and the carotid arteries were perfused with 4% paraformaldehyde/PBS. Each injured left carotid artery was excised from the proximal edge of the omohyoid muscle to the carotid bifurcation. The middle third of the segment was isolated for subsequent analyses.

Generation of Recombinant Adenovirus (Ad) Expressing Vasorin. Replication-incompetent Ads expressing vasorin-Flag (Ad-vasorin) were prepared by using the Adeno-X system (Clontech) according to the manufacturer's instructions. Viral titer was measured by end-point dilution assay by using 293 cells.

Statistical Analysis. Quantitative values are expressed as the mean ± SD. Comparisons of means were made by using Student's *t* test for unpaired values; when >2 means were compared, an ANOVA with repeated measurements was used. If a significant *F* value was found, the Scheffé post hoc test for multiple comparisons was used to identify any differences among groups.

Results

Cloning of *Vasorin*. We screened a human heart cDNA library, by using SST-REX (ref. 3 and Table 1, which is published as supporting information on the PNAS web site), and identified a type I membrane protein of 673 aa (Fig. 1*A*). The extracellular region was composed of a putative hydrophobic signal sequence, 10 tandem arrays of a leucine-rich repeat (LRR), an epidermal growth factor (EGF)-like domain, and a fibronectin type III-like domain, and the short intracellular region contained no obvious signaling domain (Fig. 1 *A* and *B*). We termed this protein vasorin, based on the expression pattern described below. By using human vasorin as a probe, we identified homologous mouse and rat protein sequences in the EMBL/GenBank/DDBJ database (accession nos. AK012169 and XM 220168, respectively).

To observe the subcellular localization of vasorin, we stained CHO cells expressing human vasorin-Flag with an anti-Flag antibody (Fig. 1*C*), and confirmed this molecule to be expressed on the cell-surface membrane. Western blotting of cell lysates from CHO stable transfectants revealed a ≈110-kDa protein (Fig. 1*D*), which was larger than the predicted molecular mass. To determine whether this increase in molecular mass was due in part to N-linked glycosylation, immunoprecipitates of vasorin were treated with N-glycosydase F. An apparent shift in molecular mass of vasorin was observed, suggesting that vasorin is a cell-surface glycoprotein (Fig. 1*D*). Next, we examined the supernatant from CHO cells expressing human vasorin-Flag, and soluble vasorin was also detected (Fig. 1*D*).

***Vasorin* Is Predominantly Expressed in VSMCs.** Tissue distribution of *vasorin* was examined by using Northern blot analysis of adult human tissues. The highest expression was detected in the aorta, and moderate expression was detected in the kidney and placenta (Fig. 1*E*). We also performed Northern analysis of various human cell lines. Interestingly, *vasorin* was not expressed abundantly in any cell lines we examined (Fig. 6, which is published as supporting information on the PNAS web site).

To determine the expression pattern of *vasorin* within the aorta, we performed *in situ* hybridization analyses. By using the antisense probe, strong expression of *vasorin* was detected in the tunica media of the proximal ascending aorta (Fig. 2*A*), the descending thoracic aorta (Fig. 2*B*), the abdominal aorta (Fig. 2*C*), and the coronary arteries (Fig. 2 *E* and *F*), suggesting that *vasorin* is expressed in VSMCs of different origins. We also performed *in situ* hybridization analyses in the kidney. *Vasorin* expression was detected in interstitial cells (Fig. 2 *G* and *H*).

Developmental Regulation of *Vasorin* Expression. The developmental regulation of *vasorin* was investigated by using Northern blot and *in situ* hybridization analyses of staged mouse embryos. As shown in Fig. 3*A*, *vasorin* mRNA expression was detected in embryonic day (E)10.5 embryos, with increasing levels of expression observed at subsequent stages (E13.5 and E17.5). With *in situ* hybridization analyses, we examined the expression pattern of *vasorin* during aortic development (Fig. 3*B*). The expression of *vasorin* increased gradually in parallel with the differentiation of VSMCs in aortas at different stages of development (E11.5, E13.5, and E17.5).

When VSMCs are established in culture, a rapid transition from a contractile differentiated phenotype to a synthetic dedifferentiated phenotype occurs (5). To investigate the influence of this phenotypic modulation on the expression of *vasorin*, semiquantitative RT-PCR was performed to compare the expression of *vasorin* in the adult rat aorta with that in cultured rat aortic VSMCs. The expression of *vasorin* was significantly downregulated in the cultured VSMCs (Fig. 3*C*).

P19 embryonal carcinoma cells differentiate into SMCs when given retinoic acid (RA) treatment. Recently, this *in vitro* differentiation system was improved by generating stable cell lines of P19 carrying a smooth muscle α-actin promoter/puromycin resistance gene cassette to enrich SMC lineage cells, by using RA plus puromycin selection. One such stable line, designated as A404, shows a high propensity for SMC differentiation even before puromycin selection (7). As expected, *vasorin* gene expression was induced by RA-treatment in A404 cells (Fig. 3*D*).

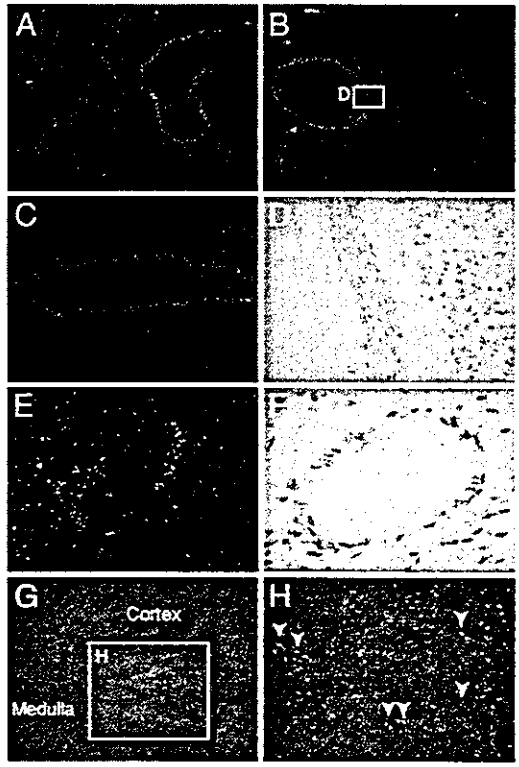

Fig. 2. *In situ* hybridization analysis of *vasorin*. Sections of adult mouse aorta at different levels (*A–D*), the coronary artery (*E* and *F*), and the kidney (*G* and *H*) are shown. *Vasorin* is expressed in VSMCs of different origins. White spots represent hybridization signals. (*A*) The proximal ascending aorta. (*B*) The descending thoracic aorta. (*C*) The abdominal aorta. (*D*) Partial magnification of bright-field image of *B*. Black spots within the elastic fibers represent hybridization signals. (*E*) The coronary artery. (*F*) A bright-field image of the coronary artery. Black spots represent hybridization signals. (*G*) The kidney. (*H*) Partial magnification of *G*. *Vasorin* is expressed in interstitial cells.

Vasorin Directly Binds to TGF-β and Modulates TGF-β Signaling *in Vitro*. An LRR, an EGF-like domain, and a fibronectin type III-like domain are characteristic motifs involved in protein–protein interactions (8). To clarify biological functions of vasorin, we generated recombinant vasorin-Fc fusion protein (Fig. 4*A*), and searched for binding partners of vasorin by using vasorin-Fc as a probe. When comparing the extracellular domain of vasorin with the EMBL/GenBank/DDBJ database, several other LRR protein family members, including decorin, were found to share a significant homology with vasorin. Decorin is a small leucine-rich proteoglycan that interacts directly with TGF-β (9, 10). Considering that vasorin has the same number of LRRs as decorin, and that TGF-β plays an important role in vascular pathophysiology, we tested whether TGF-β binds directly to vasorin. By using a surface plasmon resonance biosensor, we found that the extracellular domain of vasorin directly binds to TGF-β1 in a specific and significant manner (Fig. 4 *B* and *C*). The equilibrium dissociation constant (K_d) was calcu-

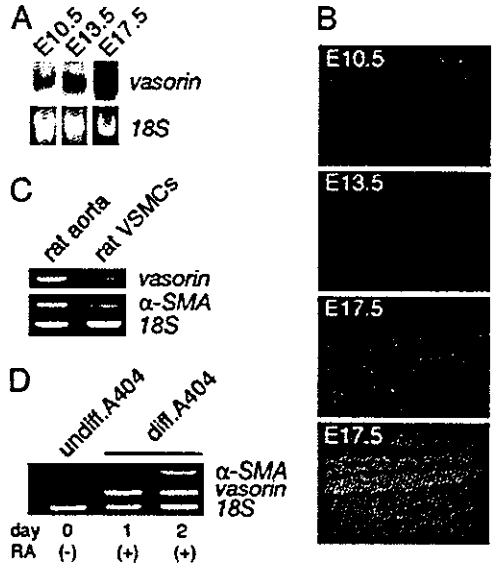

Fig. 3. Developmental regulation of *vasorin*. (*A*) Northern blot analysis of staged mouse embryos (E10.5, E13.5, and E17.5). (*B*) Expression pattern of *vasorin* during aortic development examined by *in situ* hybridization analyses. The fourth image is the corresponding bright-field image of the third representation. Arrowheads indicate the aorta in the mouse embryo (E17.5). (*C*) Semiquantitative RT-PCR comparing the expression of *vasorin* in the adult rat aorta with that in cultured rat aortic VSMCs. Rat α-smooth muscle actin (α-SMA) and 18S rRNA were used as a positive and an internal control, respectively. (*D*) Semiquantitative RT-PCR showing the induction of the *vasorin* gene in RA-treated A404 cells. Rat α-SMA and 18S rRNA were used as a positive and an internal control, respectively.

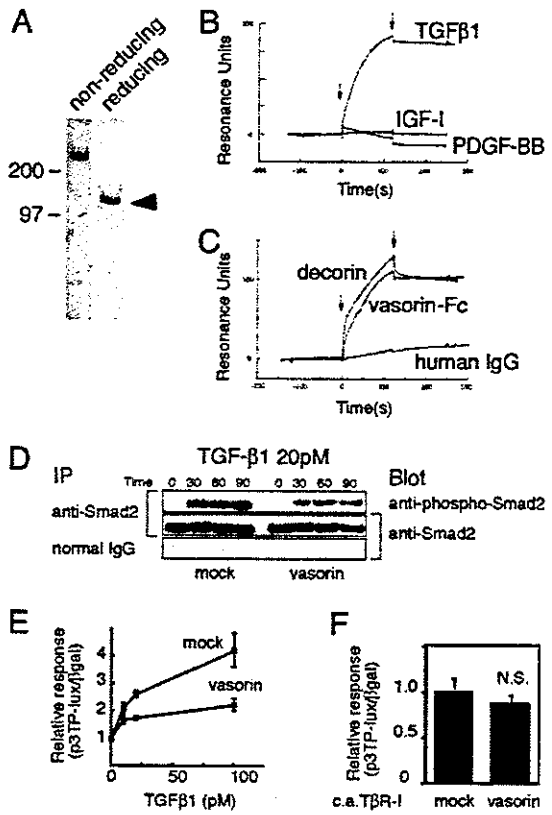

Fig. 4. Vasorin directly binds to TGF-β and modulates TGF-β signaling *in vitro*. (*A*) Purified recombinant vasorin-Fc fusion protein was free of protein contamination, as estimated by SDS/PAGE, followed by Coomassie blue staining. (*B*) Sensorgrams obtained from injection of vasorin-Fc on immobilized TGF-β1, PDGF-BB, and insulin-like growth factor I (IGF-I) are shown. (*C*) Sensorgrams obtained from injection of vasorin-Fc, decorin, and human IgG on immobilized TGF-β1 are shown. Arrowheads indicate initiation and termination of injections. (*D*) TGF-β-induced Smad2 phosphorylation was significantly inhibited in vasorin-expressing cells. Stable transfectants were treated with TGF-β1 (20 pM), and then immunoprecipitated with an anti-Smad2/3 antibody, followed by blotting with an anti-phospho-Smad2 antibody. (*E*) A reporter assay was performed by using the TGF-β-responsive reporter p3TP-lux. Stable transfectants were stimulated with TGF-β1 at various concentrations, and vasorin inhibited TGF-β-induced reporter gene activation. (*F*) Vasorin inhibited TGF-β signaling at the extracellular and/or cell-surface level. The p3TP-lux reporter and the constitutively active TβR-I were cotransfected into stable transfectants. Transfection of the constitutively active TβR-I activated the p3TP-lux reporter, but vasorin did not significantly inhibit this activation. N.S., not significant.

lated to be 0.86 nM. We also tested the binding of TGF-β2 and TGF-β3 to vasorin. TGF-β2 and TGF-β3 showed a specific binding to vasorin with a similar binding affinity to that of TGF-β1 (data not shown).

Next, we examined the functional role of vasorin in TGF-β signaling. First, stable transfectants expressing vasorin were stimulated by TGF-β1 (20 pM). Cells expressing vasorin showed a significant reduction in Smad2 phosphorylation (Fig. 4*D*). Second, we did a reporter assay, by using the TGF-β-responsive reporter p3TP-lux. TGF-β1 activated this reporter in a dose-dependent manner, and vasorin significantly inhibited this effect (Fig. 4*E*). This inhibitory effect of vasorin was specific to TGF-β signaling because vasorin did not affect the cellular responses to irrelevant cytokine stimulation (data not shown). Stable transfectants were also stimulated by using the constitutively active TGF-β type I receptor (constitutively active TβR-I) instead of TGF-β1 stimulation. Transfection of constitutively active TβR-I activated the p3TP-lux reporter, but vasorin did not significantly inhibit this activation (Fig. 4*F*). These findings indicate that vasorin inhibits TGF-β signaling at the extracellular and/or cell-surface level.

Vasorin Expression Was Down-Regulated During Vessel Repair After Arterial Injury, and Reversal of Vasorin Down-Regulation, by Using Ad-Mediated *in Vivo* Gene Transfer, Significantly Reduced Neointimal Formation at Least in Part by Modulating TGF-β Signaling in the Vessel Wall. To investigate *in vivo* functions of vasorin, we used a rat arterial balloon-injury model, because it is a well characterized atherosclerosis model of VSMC-derived lesions, and it is well established that TGF-β contributes to neointimal formation by promoting fibrosis.

Adult rats were subjected to balloon injury with a catheter inserted through the external carotid artery. Vascular injury provokes fibroproliferative activity in quiescent VSMCs, and the phenotypic modulation of VSMCs is induced. Because the fibroproliferative activity of VSMCs peaks at 3 days after injury (6), balloon-injured carotid arteries were harvested at 3 days after insertion to examine the expression levels of *vasorin* by semiquantitative RT-PCR. Consistent with our findings described above (Fig. 3 *A–D*), down-regulation of *vasorin* expression was induced by mechanical vascular injury (Fig. 5*A*). In contrast, the expression of several cytokines, including TGF-β, was up-regulated by vascular injury, and the ratio of TGF-β to vasorin was increased (Fig. 5*A*).

Next, we investigated the functional role of vasorin down-regulation in neointimal formation. To restore *vasorin* expression during vessel repair after injury, we did Ad-mediated *vasorin* gene transfer to balloon-injured rat carotid arteries. Replication-defective Ad-vasorin were constructed, and after denudation with a balloon catheter, the vessel wall was exposed to the adenoviral solution (1×10^9 pfu) for 20 min to deliver *vasorin* gene locally. First, arteries were harvested 3 days after-

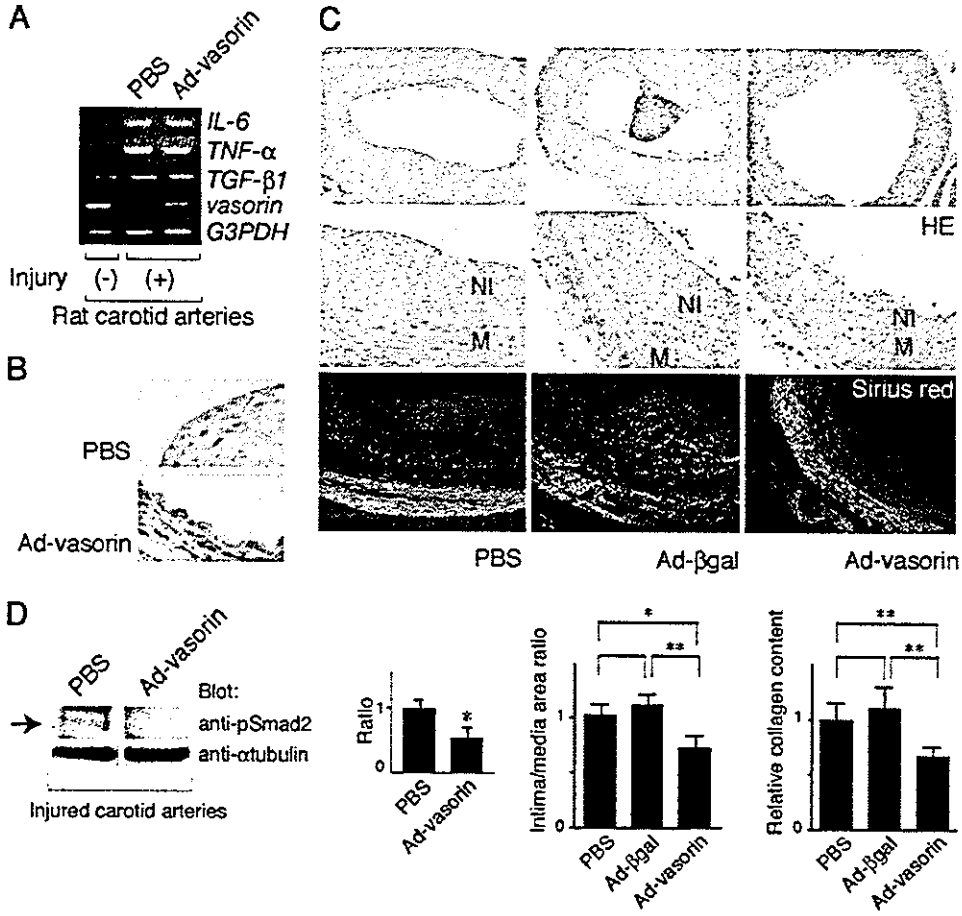

Fig. 5. Vasorin expression was down-regulated during vessel repair after arterial injury, and reversal of vasorin down-regulation significantly reduced neointimal formation, at least in part, by attenuating TGF-β signaling *in vivo*. (*A*) Rat carotid arteries were harvested at 3 days after injury to examine the expression levels of *vasorin* by semiquantitative RT-PCR analysis. Down-regulation of *vasorin* expression was induced by mechanical vascular injury, and Ad-vasorin treatment partially reversed this down-regulation. In contrast to vasorin, the expression of TGF-β1, TNF-α, and IL-6 was up-regulated by vascular injury and was not altered by vasorin administration. GAPDH was used as an internal control. (*B*) Vessels treated with Ad-vasorin were harvested 3 days afterward and were subjected to immunostaining to confirm protein expression by using the anti-Flag antibody. (*C*) Effects of Ad-vasorin on neointimal formation in rat carotid arteries at 14 days after injury ($n = 5$ arteries for each group). Representative hematoxylin/eosin-stained cross sections (*Top* and *Middle*) and Sirius red-stained cross sections (*Bottom*) of balloon-injured arteries treated with PBS (*Left*), Ad-β-galactosidase (*Center*), and Ad-vasorin (*Right*) are shown. (*Middle*) Partial magnifications of the respective *Top* images. Ad-vasorin administration significantly reduced the intima/media area ratio of injured arteries and collagen content in the lesions ($P < 0.01$), as compared with Ad-β-galactosidase administration. NI, neointima; M, media; HE, hematoxylin/eosin. *, $P < 0.05$; **, $P < 0.01$. (*D*) The inhibitory effects of vasorin administration on TGF-β signaling *in vivo*. Arteries were harvested 3 days after injury and were subjected to Western blot analysis by using the anti-phospho-Smad2 antibody. Representative data are shown. Smad2 phosphorylation was significantly reduced in all Ad-vasorin-treated arteries ($P < 0.05$). The blots were stripped and reprobed with the anti-α-tubulin antibody to ensure equal loading of proteins. The relative intensities of phospho-Smad2 bands were measured by densitometric scanning from three independent experiments. *, $P < 0.05$.

ward to examine the expression of vasorin by RT-PCR analysis (Fig. 5*A*), immunostaining (Fig. 5*B*), and Western blot analysis (data not shown). Ad-mediated *vasorin* gene transfer was successful (Fig. 5 *A* and *B*), and the expression of TGF-β, TNF-α, and IL-6 was not altered by vasorin administration (Fig. 5*A*). Second, arteries were harvested to assess the effect of *vasorin* gene transfer on neointimal formation ($n = 5$ arteries for each group) at 14 days after injury. The administration of Ad-vasorin significantly reduced the intima/media area ratio of injured arteries by 35% ($P < 0.01$), as compared with the administration of Ad-β-galactosidase (Fig. 5*C*), suggesting that restoration of vasorin expression had a significant inhibitory effect on neointimal formation. Because TGF-β stimulates extracellular matrix protein synthesis, and also functions as an antiinflammatory cytokine, we examined collagen content and leukocyte infiltration in the lesions quantitatively, by using Sirius red staining and CD45 staining, respectively. As shown in Fig. 5*C Lower*, vasorin administration significantly reduced collagen content in the lesions ($P < 0.01$), whereas leukocyte infiltration was not altered (data not shown).

Finally, we investigated whether *in vivo* vasorin administration inhibits TGF-β signaling in the vessel wall. Balloon-injured rat carotid arteries treated with Ad-vasorin were subjected to Western blot analysis, by using the anti-phospho-Smad2 antibody, when the fibroproliferative activity of VSMCs peaked (3 days after injury). Smad2 phosphorylation was significantly reduced in Ad-vasorin-treated arteries ($P < 0.05$; Fig. 5*D*). These results suggest that enhanced TGF-β signaling after vascular injury (Fig. 5*A*) is significantly inhibited by *in vivo* vasorin administration, and that vasorin inhibits neointimal formation at least in part by modulating TGF-β signaling in the vessel wall.

Discussion

VSMCs respond to various growth factors, and the best investigated situation in which VSMCs proliferate and produce extracellular matrix proteins *in vivo* is after vascular injury.

Whereas the rat carotid arterial balloon-injury model has been studied extensively, the underlying mechanisms that regulate vessel repair and neointimal formation appear to be the same in other arteries and in other species, including humans. The phenotype of VSMCs following arterial injury is similar to that observed during embryonic angiogenesis, and molecular mechanisms that regulate VSMC differentiation during embryonic development are thought to be recapitulated during vessel repair. *Vasorin* gene expression was developmentally regulated (Fig. 3 *A–D*), and, consistent with this finding, *vasorin* was down-regulated during vessel repair after arterial injury (Fig. 5*A*). This finding suggests its involvement in injury-induced vascular lesion formation. Therefore, we explored the *in vivo* functions of vasorin, by using a rat arterial balloon-injury model combined with Ad-mediated *in vivo* gene transfer. As shown in Fig. 5*C*, reversal of vasorin down-regulation had a significant inhibitory effect on neointimal formation. These results indicate that down-regulation of vasorin expression contributes to the fibroproliferative response to vascular injury.

Numerous factors that regulate VSMC activity have been studied in the arterial-injury model, and the results of these investigations suggest the importance of pathological extracellular stimuli, such as the renin-angiotensin system, catecholamines, EGF, platelet-derived growth factor (PDGF), insulin-like growth factor I, endothelin 1, TGF-β, and oxidative stress. TGF-β is a context-dependent pleiotropic cytokine, which plays a key role in the vascular response to injury. Several studies using gene transfer techniques have shown that locally enhanced TGF-β signaling enables matrix-rich neointima to develop in uninjured normal arteries of rats (11, 12). In contrast, localized blockade of TGF-β signaling results in the inhibition of neointimal formation, accompanied by reduced extracellular matrix synthesis in a rat balloon-injury model (13, 14). Of clinical relevance is the observation that the expression levels of TGF-β mRNA in restenotic lesions are higher than those in primary atherosclerotic lesions (15). These investigations indicate that TGF-β functions as a fibrogenic cytokine in a balloon-injury model, and apparently aggravates neointimal formation by promoting fibrosis. In this paper, we found that vasorin directly binds to TGF-β and negatively modulates TGF-β signaling in the vessel wall (Figs. 4 and 5*D*). Considering the functional role of TGF-β in this model, it is reasonably assumed that the *in vivo* phenotype induced by Ad-vasorin administration is mediated at least in part by the inhibitory effects of vasorin on TGF-β signaling in the vessel wall.

The extracellular region of vasorin is composed of ten tandem arrays of an LRR, an EGF-like domain, and a fibronectin type III-like domain, that are known to be involved in protein–protein interactions (Fig. 1*B*). Secreted and cell-surface molecules containing those domains, such as extracellular matrix proteins and adhesion molecules, sometimes have multiple binding partners. PDGF and TGF-β are prominent growth factors that have been suggested to play an important role in neointimal formation after arterial injury, and we demonstrated here that vasorin directly binds to TGF-β, but not to PDGF (Fig. 4*B*). However, it is possible that vasorin has other binding partners and that vasorin affects not only TGF-β signaling but also other signaling pathways, through another yet-to-be-identified mechanism. Further investigations will be needed to clarify these issues.

In the present study, we found that down-regulation of vasorin expression was induced by acute vascular injury, and that reversal of vasorin down-regulation during vessel repair inhibits neointimal formation, at least in part, by modulating cellular responses to TGF-β. These data raise a possibility that the gene expression profile of cell-surface molecules is changed by mechanical vascular injury, and that altered cellular responses to growth factors in dedifferentiated VSMCs are in part due to this change. Thus, identification and modification of the pivotal gene expression of cell-surface molecules in VSMCs may be a potential therapeutic approach to vascular fibroproliferative disorders.

We thank Dr. G. K. Owens for A404 cells, M. Ohara for language assistance, and Drs. H. Ono and H. Ogasawara for valuable advice. This work was also supported in part by grants from the Ministry of Education, Science, Technology, Sports, and Culture of Japan. The Division of Hematopoietic Factors was supported in part by the Chugai Pharmaceutical Company, Ltd.

1. Tashiro, K., Tada, H., Heilker, R., Shirozu, M., Nakano, T. & Honjo, T. (1993) *Science* **261**, 600–603.
2. Klein, R. D., Gu, Q., Goddard, A. & Rosenthal, A. (1996) *Proc. Natl. Acad. Sci. USA* **93**, 7108–7113.
3. Kojima, T. & Kitamura, T. (1999) *Nat. Biotechnol.* **17**, 487–490.
4. Nosaka, T., Kawashima, T., Misawa, K., Ikuta, K., Mui, A. L. & Kitamura, T. (1999) *EMBO J.* **18**, 4754–4765.
5. Chamley-Campbell, J., Campbell, G. R. & Ross, R. (1979) *Physiol. Rev.* **59**, 1–61.
6. Clowes, A. W., Reidy, M. A. & Clowes, M. M. (1983) *Lab. Invest.* **49**, 327–333.
7. Manabe, I. & Owens, G. (2001) *Circ. Res.* **88**, 1127–1134.
8. Kajava, A. V. (1998) *J. Mol. Biol.* **277**, 519–527.
9. Iozzo, R. V. (1999) *J. Biol. Chem.* **274**, 18843–18846.
10. Yamaguchi, Y., Mann, D. M. & Ruoslahti, E. (1990) *Nature* **346**, 281–284.
11. Nabel, E. G., Shum, L., Pompili, V. J., Yang, Z. Y., San, H., Shu, H. B., Liptay, S., Gold, L., Gordon, D., Derynck, R., *et al.* (1993) *Proc. Natl. Acad. Sci. USA* **90**, 10759–10763.
12. Schulick, A. H., Taylor, A. J., Zuo, W., Qiu, C. B., Dong, G., Woodward, R. N., Agah, R., Roberts, A. B., Virmani, R. & Dichek, D. A. (1998) *Proc. Natl. Acad. Sci. USA* **95**, 6983–6988.
13. Yamamoto, K., Morishita, R., Tomita, N., Shimozato, T., Nakagami, H., Kikuchi, A., Aoki, M., Higaki, J., Kaneda, Y. & Ogihara, T. (2000) *Circulation* **102**, 1308–1314.
14. Kingston, P. A., Sinha, S., David, A., Castro, M. G., Lowenstein, P. R. & Heagerty, A. M. (2001) *Circulation* **104**, 2595–2601.
15. Nikol, S., Isner, J. M., Pickering, J. G., Kearney, M., Leclerc, G. & Weir, L. (1992) *J. Clin. Invest.* **90**, 1582–1592.

Cardiomyocytes fuse with surrounding noncardiomyocytes and reenter the cell cycle

Katsuhisa Matsuura,[1,2] Hiroshi Wada,[1] Toshio Nagai,[1] Yoshihiro Iijima,[1] Tohru Minamino,[1] Masanori Sano,[1] Hiroshi Akazawa,[1] Jeffery D. Molkentin,[3] Hiroshi Kasanuki,[2] and Issei Komuro[1]

[1]Department of Cardiovascular Science and Medicine, Chiba University Graduate School of Medicine, Chiba 260-8670, Japan
[2]Department of Cardiology, The Heart Institute of Japan, Tokyo Women's Medical University, Tokyo 162-8666, Japan
[3]Division of Molecular Cardiovascular Biology, Department of Pediatrics, Cincinnati Children's Hospital Medical Center, Cincinnati, OH 45229

The concept of the plasticity or transdifferentiation of adult stem cells has been challenged by the phenomenon of cell fusion. In this work, we examined whether neonatal cardiomyocytes fuse with various somatic cells including endothelial cells, cardiac fibroblasts, bone marrow cells, and endothelial progenitor cells spontaneously in vitro. When cardiomyocytes were cocultured with endothelial cells or cardiac fibroblasts, they fused and showed phenotypes of cardiomyocytes. Furthermore, cardiomyocytes reentered the G2-M phase in the cell cycle after fusing with proliferative noncardiomyocytes. Transplanted endothelial cells or skeletal muscle–derived cells fused with adult cardiomyocytes in vivo. In the cryo-injured heart, there were Ki67-positive cells that expressed both cardiac and endothelial lineage marker proteins. These results suggest that cardiomyocytes fuse with other cells and enter the cell cycle by maintaining their phenotypes.

Introduction

Many reports have indicated that adult stem cells have "plasticity" and transdifferentiate into various types of cells including cardiomyocytes (Jackson et al., 2001; Orlic et al., 2001a; Badorff et al., 2003). Bone marrow cells have been incorporated into the damaged myocardium and have expressed cardiac-specific proteins (Jackson et al., 2001; Orlic et al., 2001a; Mangi et al., 2003). Besides undifferentiated stem cells, differentiated somatic cells such as endothelial cells and skeletal muscle–derived cells have been also reported to transdifferentiate into cardiomyocytes when cocultured with cardiomyocytes (Condorelli et al., 2001; Iijima et al., 2003). However, the concept of plasticity has been challenged by the new findings that embryonic stem cells adopt the phenotype of bone marrow cells or central nervous stem cells by cell fusion (Terada et al., 2002; Ying et al., 2002). Bone marrow cells have been reported to fuse with hepatocytes in the severely injured liver and proliferate extensively, resulting in millions of highly aneuploid new hepatocytes (Vassilopoulos et al., 2003; Wang et al., 2003). In the brain, bone marrow cells form stable heterokaryons with Purkinje neurons in the absence of selective pressure. In this intracellular milieu, bone marrow cell–derived nuclei are reprogrammed to activate the Purkinje-specific gene, resulting in the phenotype of the Purkinje cells becoming dominant over time (Weimann et al., 2003). These results suggest that cell fusion might be one of the physiological mechanisms through which the cells change their lineage and the tissues are rejuvenated or regenerated.

Adult cardiomyocytes have been thought to be terminally differentiated and unable to divide, thus myocyte growth under pathologic conditions as well as physiologic conditions is believed to be accomplished only by cellular hypertrophy (Morgan and Baker, 1991; Chien, 1995). Cytoplasmic extracts of adult cardiomyocytes have been reported to reduce the expression of proliferating cell nuclear antigens in proliferating noncardiomyocytes (Engel et al., 2003), suggesting that some inhibitory molecules of the cell cycle might exist in the cytoplasm of adult cardiomyocytes. However, recent reports have indicated that adult cardiomyocytes can divide after myocardial infarction and at end-stage heart failure (Kajstura et al., 1998; Beltrami et al., 2001). The precise mechanism of how cardiomyocytes acquire proliferative ability is still elusive, but there is a possibility that mobilized bone marrow–derived stem cells or cardiac progenitor cells start to proliferate in response to some environmental cues (Orlic et al., 2001b; Beltrami et al.,

K. Matsuura and H. Wada contributed equally to this paper.

The online version of this article includes supplemental material.

Correspondence to Issei Komuro: komuro-tky@umin.ac.jp

Abbreviations used in this paper: ANF, atrial natriuretic factor; β-gal, β-galactosidase; CAT, chloramphenicol acetyltransferase; cFB, cardiac fibroblasts; cTnT, cardiac troponin T; EPC, endothelial progenitor cell; HUVEC, human umbilical vein endothelial cells; PH3, phosphohistone H3; RFP, red fluorescent protein; UEA-1, ulex europaeus agglutinin-1; vWF, von Willebrand factor.

© The Rockefeller University Press $8.00
The Journal of Cell Biology, Vol. 167, No. 2, October 25, 2004 351–363
http://www.jcb.org/cgi/doi/10.1083/jcb.200312111

Supplemental Material can be found at:
http://www.jcb.org/cgi/content/full/jcb.200312111/DC1

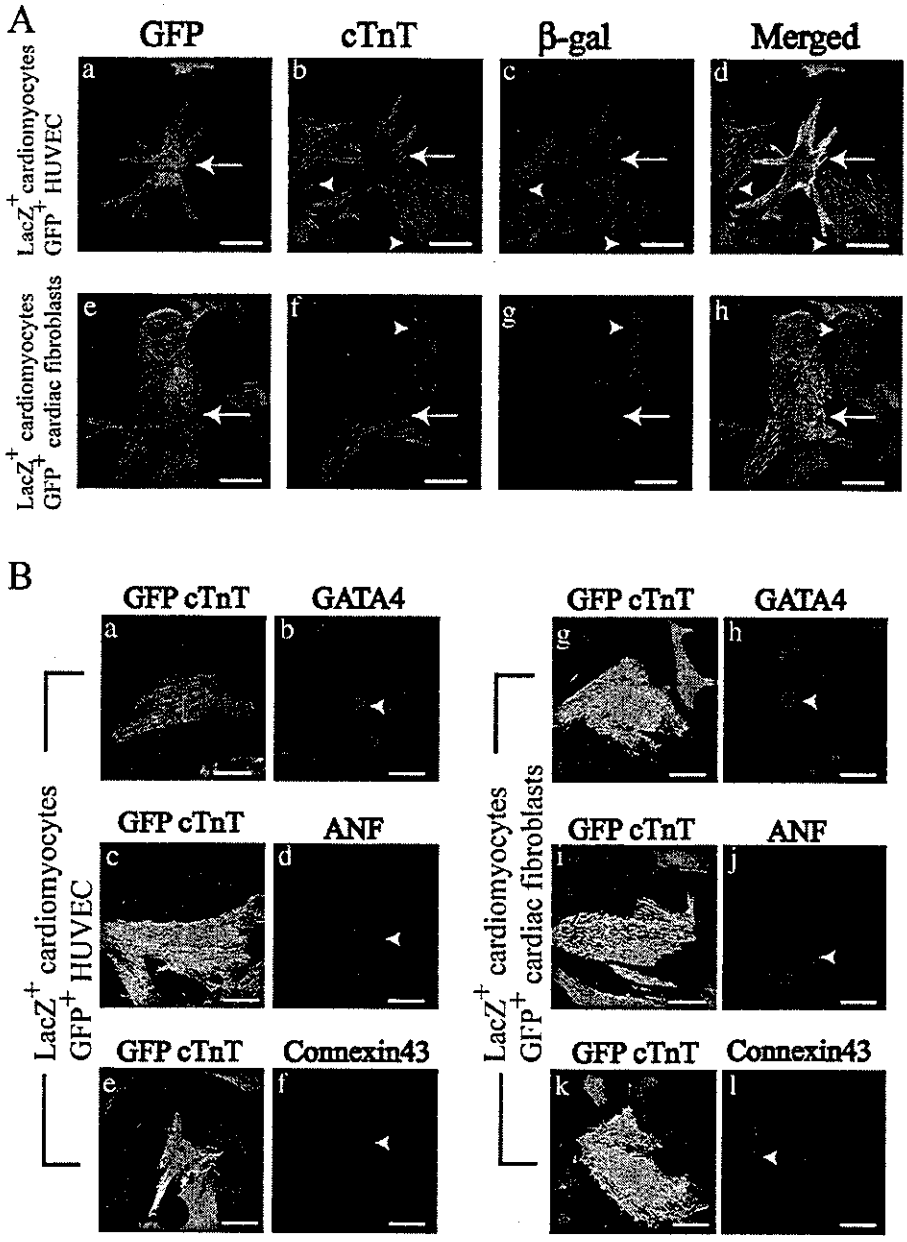

Figure 1 **HUVEC and cFB acquired the cardiac phenotype through cell fusion with cardiomyocytes.** (A) *LacZ*-expressing cardiomyocytes of neonatal rats were cocultured with GFP HUVEC (a-d) or GFP cFB (e-h) and stained with mouse monoclonal anti-cTnT (red) and rabbit polyclonal anti-β-gal (blue). Merged images were obtained from the same confocal plane. GFP HUVEC and GFP cFB (a and e, arrow) expressed cTnT (b and f, arrow) and β-gal (c and g, arrow) in the same cell (merged on d and h). Arrowheads indicate the nonfused cardiomyocytes. (B) *LacZ*-expressing cardiomyocytes of neonatal rats were cocultured with GFP HUVEC (a-f) or GFP cFB (g-l) and stained with mouse monoclonal anti-cTnT (red) and goat polyclonal anti-GATA4 or rabbit polyclonal anti-ANF or anti-connexin43 antibodies (blue). HUVEC and GFP cTnT-expressing GFP cFB (g, i, and k) expressed GATA4 (b and h, arrowhead), ANF (d and j, arrowhead), and connexin43 (f and l, arrowhead)

2003; Matsuura et al., 2004). Recently, Oh et al. have shown which the ability to proliferate might be reported that transplanted cardiac progenitor cells can become cardiomyocytes by surrounding proliferative nonc murine heart not only differentiate into cardiomyocytes, but also fuse with preexisting cardiomyocytes in the diseased heart. To the best of our knowledge, no studies have been reported regarding the cell model. This finding indicates that there is another possible fusion between cardiomyocytes and noncardiomyocytes. Evans e

THE JOURNAL OF BIOLOGICAL CHEMISTRY
© 2004 by The American Society for Biochemistry and Molecular Biology, Inc.

Vol. 279, No. 39, Issue of September 24, pp. 41095–41103, 2004
Printed in U.S.A.

Diphtheria Toxin-induced Autophagic Cardiomyocyte Death Plays a Pathogenic Role in Mouse Model of Heart Failure*

Received for publication, December 1, 2003, and in revised form, May 20, 2004
Published, JBC Papers in Press, July 22, 2004, DOI 10.1074/jbc.M313084200

Hiroshi Akazawa‡§, Shinji Komazaki¶, Hiroaki Shimomura¶, Fumio Terasaki‖, Yunzeng Zou‡, Hiroyuki Takano‡, Toshio Nagai‡, and Issei Komuro‡**

From the ‡Department of Cardiovascular Science and Medicine, Chiba University Graduate School of Medicine, 1-8-1 Inohana, Chuo-ku, Chiba 260-8670, Japan, the ¶Department of Anatomy, Saitama Medical School, 38 Morohongou, Moroyama, Iruma 350-0495, Japan, ‖The Third Division, Department of Internal Medicine, Osaka Medical College, 2-7 Daigaku-machi, Takatsuki 569-8686, Japan, and the §Foundation for Biomedical Research and Innovation, 6-1, Minatojima Nakamachi, Chuo-ku, Kobe 650-8543, Japan

It is still not clear whether loss of cardiomyocytes through programmed cell death causes heart failure. To clarify the role of cell death in heart failure, we generated transgenic mice (TG) that express human diphtheria toxin receptor in the hearts. A mosaic expression pattern of the transgene was observed, and the transgene-expressing cardiomyocytes (17.3% of the total cardiomyocytes) were diffusely scattered throughout the ventricles. Intramuscular injection of diphtheria toxin induced complete elimination of the transgene-expressing cardiomyocytes within 7 days, and ~80% of TG showed pathophysiological features characteristic of heart failure and were dead within 14 days. Degenerated cardiomyocytes of the TG heart showed characteristic features indicative of autophagic cell death such as up-regulated lysosomal markers and abundant autophagosomes containing cytosolic organelles like cardiomyocytes of human dilated cardiomyopathy. The heart failure-inducible TG are a useful model for dilated cardiomyopathy, and provided evidence indicating that myocardial cell loss through autophagic cell death plays a causal role in the pathogenesis of heart failure.

Cardiomyocyte death is observed in a number of pathological conditions such as ischemic or dilated cardiomyopathy, hypertensive heart disease, and aging (1). Oncosis has been recognized to be a principal mechanism of myocardial cell death, but during the last decade, much emphasis has been put on the importance of apoptosis on the basis of detectable apoptotic cardiomyocytes in animal and human models of heart failure (2). Recently, autophagic cell death (ACD)[1] has been demonstrated as another type of myocardial cell death in human failing hearts (3–7). Although a decline in pumping capacity initiated by cardiomyocyte loss is supposed to induce ventricular remodeling and finally results in symptomatic heart failure (8), there still remains a controversy over the pathogenic role of cell death in progression of heart failure (9, 10). An intractable problem that hampers mechanistic insights is the low occurrence of myocardial cell death in failing hearts, although it differs strikingly according to the models examined and technical specificity (2, 8). Furthermore, in human hearts, most samples were obtained from patients with end-stage heart failure who underwent heart transplantation and thus it remains unknown whether myocardial cell death occurs persistently from an early stage and is causative to progression of heart failure (8). To circumvent these obstacles, we established an inducible heart failure mouse model utilizing diphtheria toxin (DT)-mediated cell ablation, in which a given number of cardiomyocytes are arbitrarily and synchronously ablated, and prospective and serial analysis is available.

DT is a two-peptide protein consisting of fragments A (DT-A) and B (DT-B) produced by *Corynebacterium diphtheriae* (11). DT binds to the DT receptor on the cell surface through DT-B and is internalized into acidic endocytic vesicles, which allows release of catalytic DT-A into the cytoplasm (12). DT-A exerts its cytotoxicity by ADP-ribosylating elongation factor 2 and thereby inhibiting protein synthesis in infected cells (13). DT receptor has been identified as a precursor of heparin-binding EGF-like growth factor (pro-HB-EGF) (14, 15). Intriguingly, DT cannot bind to rodent pro-HB-EGF because of substitution of amino acids required for DT binding, whereas primate pro-HB-EGF acts as a functional DT receptor (16). Therefore, specific cells in mice are ideally sensitized to DT by forced expression of human pro-HB-EGF (17).

To enable cardiac-specific cell ablation, we generated transgenic mice (TG) expressing human pro-HB-EGF in the hearts under the control of *α-myosin heavy chain* promoter. Administration of DT induced ablation of transgene-expressing cardiomyocytes, and subsequently symptomatic heart failure. In this mouse model of heart failure, autophagy but not apoptosis was the mechanism of cardiomyocyte death. Autophagy is a dynamic process and intracellular constituents are sequestered by membranes and subsequently degradated or recycled in lysosome or vacuole (18–20). In this sense, autophagy is involved in maintaining cellular homeostasis and turnover in physiological conditions. However, a growing body of evidence suggests that autophagy is implicated in execution of pro-

* This work was supported in part by grants from the Japanese Ministry of Education, Science, Sports, and Culture of Japan, Japan Health Sciences Foundation, Takeda Medical Research Foundation, Takeda Science Foundation, Uehara Memorial Foundation, Kato Memorial Trust for Nambyo Research, an the Japan Medical Association (to I. K.) and a Japanese Heart Foundation/Pfizer Japan Grant on Cardiovascular Disease Research (to H. A.), and the New Energy and Industrial Technology Development Organization. The costs of publication of this article were defrayed in part by the payment of page charges. This article must therefore be hereby marked "*advertisement*" in accordance with 18 U.S.C. Section 1734 solely to indicate this fact.

** To whom correspondence should be addressed. Tel.: 81-43-226-2097; Fax: 81-43-226-2557; E mail: komuro-tky@umin.ac.jp.

[1] The abbreviations used are: ACD, autophagic cell death; BNP, brain natriuretic peptide; DT, diphtheria toxin; DT-A, DT fragment A; DT-B, DT fragment B; LAMP-1, lysosome-associated membrane protein-1; MCP-1, macrophage chemoattractant protein-1; MLP, muscle LIM protein; pro-HB-EGF, precursor of heparin-binding epidermal growth factor-like growth factor; SERCA2, sarcoplasmic reticulum calcium-ATPase 2; TG, transgenic mice; WT, wild-type mice.

grammed cell death and is closely linked to several pathological conditions (21–23). Our model of experimentally induced heart failure provided direct evidence that myocardial cell loss through ACD causes heart failure, and will be useful to dissect the molecular mechanisms underlying structural and functional changes in heart failure.

EXPERIMENTAL PROCEDURES

Generation of Transgenic Mice—Human *pro-HB-EGF* cDNA (gift from A. Ullrich, Max-Planck-Institute of Biochemistry, Martinsried, Germany) was subcloned into the α-myosin heavy chain promoter-containing expression vector (gift from J. Robbins, Children's Hospital, Cincinnati, OH). The 6.9-kb DNA fragment was microinjected as a transgene into pronuclei of eggs from BDF1 mice, and the eggs were transferred into the oviducts of pseudopregnant ICR mice. The transgene was identified by Southern blot and PCR analysis. All protocols using mice were approved by the Institutional Animal Care and Use Committee of Chiba University.

Administration of Diphtheria Toxin—Diphtheria toxin (Sigma) was reconstituted in 10 mM sodium phosphate buffer (pH 7.4) containing 5% lactose, and was administered by intramuscular injection.

Northern Blot and in Situ Hybridization Analysis—For Northern blot analysis, total RNA (20 μg) prepared from tissues were hybridized with cDNA probes. Probes for brain natriuretic peptide (*BNP*), skeletal α-actin, sarcoplasmic reticulum calcium-ATPase 2 (*SERCA2*), and *TNF-α* were previously described (24–26). Probes for macrophage chemoattractant protein-1 (*MCP-1*) and collagens (*Col1a2* and *Col3a1*) were gifts from K. Matsushima (Universitty of Tokyo, Tokyo, Japan) and S. Kim (Osaka City University, Osaka, Japan), respectively. Digoxygenin-labeled riboprobes were synthesized by using the 0.7-kb human *pro-HB-EGF* cDNA, and RNA *in situ* hybridization was performed as described previously (27).

Western Blot Analysis—Protein samples were fractionated by SDS-PAGE, and immunoblot analysis was performed as described previously (26, 28).

Transthoracic Echocardiography—Mice were anesthetized by intraperitoneal injection of a mixture of ketamine (100 mg/kg) and xylazine (5 mg/kg). Cardiac function was evaluated with echocardiography (SONOS 4500, Philips, Eindhoven, the Netherlands) using a 12-MHz transducer as described previously (26).

Histological Analysis and Immunohistochemistry—Hearts were fixed in 10% neutralized formalin and embedded in paraffin. Serial sections at 5 μm were routinely stained with hematoxylin-eosin for morphological analysis, and with Masson's trichrome for detection of fibrosis. For measurement of the myocyte cross-sectional area, semithin sections with silver staining were analyzed. Suitable cross-sections were defined as having round-to-oval cardiomyocyte sections and nearly round-shaped capillaries that perfused in the region. For immunohistochemistry, Vectastain ABC kit (Vector Laboratories, Burlingame, CA) was used to detect the primary antibodies. The sections were counterstained with hematoxylin.

Antibodies—The following antibodies were used: goat polyclonal anti-human HB-EGF (R&D Systems, Minneapolis, MN), anti-actin (20–33) IgG fraction of antiserum developed in rabbit (Sigma), mouse monoclonal anti-Ly-6G, mouse monoclonal anti-Mac-3, mouse monoclonal anti-CD3, mouse monoclonal anti-Bcl-xL, mouse monoclonal anti-cytochrome *c* (BD Pharmingen, San Diego, CA), rabbit polyclonal anti-caspase 3, mouse monoclonal anti-phospho-Bad, rabbit polyclonal anti-Bad (Cell Signaling, Beverly, MA), rabbit polyclonal anti-Bcl2, rabbit polyclonal anti-Bax, goat polyclonal anti-cathepsin D, rat monoclonal anti-lysosome-associated membrane protein-1 (LAMP-1), goat polyclonal anti-UBC2, goat polyclonal anti-E6-AP, goat polyclonal anti-UFD1 (Santa Cruz Biotechnology, Santa Cruz, CA), mouse monoclonal anti-COX I (Molecular Probes, Eugene, OR), mouse monoclonal anti-ubiquitin (Chemicon, Temecula, CA), and mouse monoclonal anti-E1 (Upstate, Charlottesville, VA).

Evaluation of DNA Fragmentation—TUNEL assay using paraffin sections was performed with an *in situ* apoptosis detection kit (Takara Biomedicals, Otsu, Japan). For agarose gel electrophoresis for DNA fragmentation, genome DNA (10 μg) was electrophoretically fractionated on a 1.5% agarose gel and stained with ethidium bromide as described previously (29). To induce apoptosis in spleens as positive controls, we injected lipopolysaccharide (40 mg/kg) (Sigma) in phosphate-buffered saline intraperitoneally into age-matched mice. Mice were sacrificed 12 h after lipopolysaccharide injection and spleens were excised (30).

Electronmicroscopy—Hearts were fixed in 3% paraformaldehyde, 2.5% glutaraldehyde, and 0.1 M cacodylate buffer (pH 7.4). After washing with the buffer solution and post-fixation in 1% OsO_4 and 0.1 M cacodylate buffer (pH 7.4), they were washed with the buffer solution, dehydrated using alcohol and acetone, and embedded in epoxy resin. Ultrathin sections were examined under the electron microscope (31).

Statistical Analysis—All values are expressed as mean ± S.E. Comparisons were made by Student's *t* test or one-way analysis of variance as appropriate. Values of $p < 0.05$ were considered statistically significant.

RESULTS

Inducible Myocardial Cell Ablation in TG Expressing Human DT Receptor in the Hearts—To confer DT sensitivity to cardiomyocytes in mice, we generated TG expressing human DT receptor, pro-HB-EGF, under the control of the α-myosin heavy chain promoter (Fig. 1*A*). Of two independent founder lines with successful germline transmission, one line was chosen for further analysis on the basis of transgene expression levels. By immunoblot analysis using an antibody specific for human pro-HB-EGF, we confirmed cardiac-specific expression of the transgene (Fig. 1*B*). *In situ* hybridization analysis using a specific riboprobe for human *pro-HB-EGF* further revealed a mosaic expression pattern of the transgene in the hearts (Fig. 1*C*). Expression of the transgene was scattered throughout the TG hearts, and the number of transgene-expressing cardiomyocytes was 17.3 ± 6.0% out of total cardiomyocytes.

To induce DT-mediated myocardial cell ablation, we administered DT by intramuscular injection to TG and wild-type mice (WT) at 10 weeks of age. When 5 mg/kg DT was administered, TG became lethargic and ~80% of TG died within 10 days after injection of DT, although WT appeared normal (Fig. 1*D*). Immunoblot analysis in combination with *in situ* hybridization analysis revealed that expression of human pro-HB-EGF in the TG hearts was significantly decreased on the next day of DT injection, and almost disappeared on the following day (Fig. 1*E*). After 7 days, transgene-expressing cardiomyocytes were undetected in the TG hearts, suggesting that they were completely ablated through DT-mediated cytotoxicity.

DT-mediated Myocardial Cell Loss Caused Heart Failure in Mice—We next examined the geometric, functional, and histological changes in the hearts caused by DT-mediated myocardial cell damages. Gross inspections of the TG hearts 7 days after DT injection showed global chamber dilatation with marked wall thinning and atrial thrombus (Fig. 2*A*), and the heart to body weight ratios were ~1.3-fold increased (Fig. 2*B*), whereas the mock-treated TG hearts and DT- or mock-treated WT hearts showed no geometric change (Fig. 2).

To evaluate cardiac function, we performed transthoracic echocardiographic examination. Seven days after injection, a ~1.3-fold increase in the left ventricular end-diastolic dimension and a 1.5–1.7-fold decrease in left ventricular wall thickness were observed in DT-treated TG, whereas these parameters were unchanged in mock-treated TG (Fig. 2, *C* and *D*) and DT- or mock-treated WT. Echocardiographic examination also demonstrated a 2.4-fold reduction in % FS in DT-treated TG. These results suggest that injection of DT induced deterioration of LV systolic function with chamber dilatation and ventricular wall thinning in TG. In contrast, no discernible phenotype was observed in TG in the absence of DT, and DT had no harmful effect on WT.

Hematoxylin-eosin staining of the histological sections of TG hearts 7 days after DT injection revealed degenerated cardiomyocytes surrounded by inflammatory cells (Fig. 3*A*). These pathological findings were not observed in WT with or without DT injection (data not shown). The infiltrating inflammatory cells were identified as macrophages by immunohistochemical analysis using anti-Mac-3 antibody (Fig. 3*B*). Histological sections with Masson's trichrome staining showed interstitial fibrosis in DT-treated TG hearts (Fig. 3*A*). Silver staining of the